arXiv:hep-ph/0602179 v1   20 Feb 2006

Charmonium Production at High Energy in the k_T-Factorization Approach

B.A. Kniehl[*] and D.V. Vasin[†]

II. Institut für Theoretische Physik, Universität Hamburg,

Luruper Chaussee 149, 22761 Hamburg, Germany

V.A. Saleev[‡]

Department of Physics, Samara State University,

Ac.   Pavlov St. 1, 443011 Samara, Russia

Abstract

We study charmonium production at high-energy colliders (Tevatron, HERA, and LEP2) in the framework of the k_T-factorization approach and the factorization formalism of non-relativistic quantum chromodynamics at leading order in the strong-coupling constant α_s and the relative velocity v. The transverse-momentum distributions of direct and prompt J/ψ-meson production measured at the Fermilab Tevatron are fitted to obtain the non-perturbative long-distance matrix elements for different choices of unintegrated gluon distribution functions in the proton. Using the matrix elements thus obtained, we predict charmonium production rates in $\gamma\gamma$, γp, and deep-inelastic ep collisions including the contributions from both direct and resolved photons. The results are compared with the known ones obtained in the conventional parton model and with recent experimental data from HERA and LEP2.

[*]Electronic address: kniehl@desy.de

[†]Electronic address: dmitriy.vasin@desy.de; on leave from Department of Physics, Samara State University,

Ac. Pavlov St. 1, 443011 Samara, Russia

[‡]Electronic address: saleev@ssu.samara.ru

I. INTRODUCTION

Charmonium production at high energies has provided a useful laboratory for testing the high-energy limit of quantum chromodynamics (QCD) as well as the interplay of perturbative and non-perturbative phenomena in QCD. The factorization formalism of non-relativistic QCD (NRQCD) [1] is a theoretical framework for the description of heavy-quarkonium production and decay. The factorization hypothesis of NRQCD assumes the separation of the effects of long and short distances in heavy-quarkonium production. NRQCD is organized as a perturbative expansion in two small parameters, the strong-coupling constant α_s and the relative velocity v of the heavy quarks.

The phenomenology of strong interactions at high energies exhibits a dominant role of gluon interactions in quarkonium production. In the conventional parton model [2], the initial-state gluon dynamics is controlled by the Dokshitzer-Gribov-Lipatov-Altarelli-Parisi (DGLAP) evolution equation [3]. In this approach, it is assumed that $S > \mu^2 \gg \Lambda_{\mathrm{QCD}}^2$, where $\sqrt{S}$ is the invariant collision energy, μ is the typical energy scale of the hard interaction, and Λ_{QCD} is the asymptotic scale parameter. In this way, the DGLAP evolution equation takes into account only one big logarithm, namely $\ln(\mu/\Lambda_{\mathrm{QCD}})$. In fact, the collinear approximation is used, and the transverse momenta of the incoming gluons are neglected.

In the high-energy limit, the contribution from the partonic subprocesses involving t-channel gluon exchanges to the total cross section can become dominant. The summation of the large logarithms $\ln(\sqrt{S}/\mu)$ in the evolution equation can then be more important than the one of the $\ln(\mu/\Lambda_{\mathrm{QCD}})$ terms. In this case, the non-collinear gluon dynamics is described by the Balitsky-Fadin-Kuraev-Lipatov (BFKL) evolution equation [4]. In the region under consideration, the transverse momenta (k_T) of the incoming gluons and their off-shell properties can no longer be neglected, and we deal with reggeized t-channel gluons. The theoretical framework for this kind of high-energy phenomenology is the so-called k_T-factorization approach [5, 6], which can be based on effective quantum field theory implemented with the non-abelian gauge-invariant action, as was suggested a few years ago [7].

This paper is organized as follows. In Sec. II, the k_T-factorization approach is briefly reviewed and compared with the collinear parton model. The NRQCD formalism applied to heavy-quarkonium production is briefly recapitulated in Sec. III. In Sec. IV, we present in analytic form the squared amplitudes for S- and P-wave quarkonium production via the

2

fusion of reggeized gluons at leading order (LO) in α_s and v. In Sec. V, we perform fits to the transverse-momentum (p_T) distributions of inclusive charmonium production measured at the Fermilab Tevatron to obtain numerical values for the non-perturbative matrix elements (NMEs) of the NRQCD factorization formalism. In Secs. VI and VII, we compare our theoretical predictions with recent experimental data of charmonium production in $\gamma\gamma$, γp, and deep-inelastic ep scattering at the DESY HERA and CERN LEP2 colliders. Section VIII contains our conclusions.

II.   THE k_T-FACTORIZATION APPROACH

In the phenomenology of strong interactions at high energies, it is necessary to describe the QCD evolution of the gluon distribution functions of the colliding particles starting from some scale μ_0, which controls the non-perturbative regime, to the typical scale μ of the hard-scattering processes, which is typically of the order of the transverse mass $M_T = \sqrt{M^2 + |\mathbf{p}_T|^2}$ of the produced particle (or hadron jet) with (invariant) mass M and transverse two-momentum $\mathbf{p}_T$. In the region of very high energies, the typical ratio $x = \mu/\sqrt{S}$ becomes very small, $x \ll 1$. This leads to large logarithmic contributions of the type $[\alpha_s \ln(1/x)]^n$, which need to be resummed. This is conveniently done by adopting the high-energy factorization scheme, which also known as the k_T-factorization approach, in which the incoming t-channel gluons have a finite transverse two-momentum $\mathbf{k}_T$ and are off mass shell. This implies the notion of an unintegrated gluon distribution function $\Phi(x, |\mathbf{k}_T|^2, \mu^2)$. The resummation is then implemented by the BFKL evolution equation [4].

Effective Feynman rules for processes involving incoming off-shell gluons were provided in Ref. [6]. The special trick is to choose the polarization four-vector of the incoming gluon as

$$\varepsilon^\mu(k_T) = \frac{k_T^\mu}{|\mathbf{k}_T|}, \tag{1}$$

where $k_T^\mu = (0, \mathbf{k}_T, 0)$ is the transverse four-momentum of the gluon. In the case of gluon-gluon fusion, the four-momenta of the incoming gluons can be written as

$$k_1^\mu = x_1 P_1^\mu + k_{1T}^\mu,$$
$$k_2^\mu = x_2 P_2^\mu + k_{2T}^\mu, \tag{2}$$

where $P_1^\mu = (\sqrt{S}/2)(1,0,0,1)$ and $P_2^\mu = (\sqrt{S}/2)(1,0,0,-1)$ are the four-momenta of the

colliding protons in the center-of-mass frame. In the following, we shall also use the short-hand notation $p_T = |\mathbf{p}_T|$ etc. for the absolute of the transverse two-momentum.

In Ref. [8], the incoming off-shell gluons are considered as Reggeons (or reggeized gluons), which are interacting with quarks and on-shell Yang-Mills gluons in a specific way. Recently, in Ref. [9], the Feynman rules for the effective field theory based on the non-abelian gauge-invariant action [7] were derived for the vertices RRg, Rgg, $RRgg$, $Rggg$, and $RRggg$, where R is an off-shell reggeized gluon and g is an on-shell Yang-Mills gluon. The interaction of a reggeized gluon with a quark is mediated via the transition vertex Rg. For the relevant LO amplitudes, which are calculated below, both approaches [6, 8] give the same answers. As was shown in Ref. [10], the effective vertex RRg [8] can be obtained using the prescription [6] for the off-shell gluon polarization four-vector of Eq. (1).

In the k_T-factorization approach, which is based on the high-energy limit of QCD, the hadronic cross section of quarkonium ($\mathcal{H}$) production through the process

$$p + p \rightarrow \mathcal{H} + X \tag{3}$$

and the partonic cross section for the reggeized-gluon fusion subprocess

$$R + R \rightarrow \mathcal{H} + X \tag{4}$$

are related as

$$d\sigma^{\mathrm{KT}}(p + p \rightarrow \mathcal{H} + X, S) = \int \frac{dx_1}{x_1} \int d|\mathbf{k}_{1T}|^2 \int \frac{d\varphi_1}{2\pi} \Phi(x_1, |\mathbf{k}_{1T}|^2, \mu^2)$$

$$\times \int \frac{dx_2}{x_2} \int d|\mathbf{k}_{2T}|^2 \int \frac{d\varphi_2}{2\pi} \Phi(x_2, |\mathbf{k}_{2T}|^2, \mu^2) d\hat{\sigma}(R + R \rightarrow \mathcal{H} + X, \mathbf{k}_{1T}, \mathbf{k}_{2T}, \hat{s}), \tag{5}$$

where $\hat{s} = x_1 x_2 S - (\mathbf{k}_{1T} + \mathbf{k}_{2T})^2$, $x_{1,2}$ are the fractions of the proton momenta passed on to the reggeized gluons, and $\varphi_{1,2}$ are the angles enclosed between $\mathbf{k}_{1,2T}$ and the transverse momentum $\mathbf{p}_T$ of $\mathcal{H}$, which we take to point along the x axis.

In our numerical calculations, we use the unintegrated gluon distribution functions by Blümlein (JB) [11], by Jung and Salam (JS) [12], and by Kimber, Martin, and Ryskin (KMR) [13]. A direct comparison between different unintegrated gluon distributions as functions of x, $|\mathbf{k}_T|^2$, and μ^2 may be found in Ref. [14]. Note, that the JB version is based on the BFKL evolution equation [4]. On the contrary, the JS and KMR versions were obtained using the more complicated Catani-Ciafaloni-Fiorani-Marchesini (CCFM) evolution equation [15], which takes into account both large logarithms of the types $\ln(1/x)$ and $\ln(\mu/\Lambda_{\mathrm{QCD}})$.

4

For $\mu \gg \Lambda_{\rm QCD}$ and not too small $x = \mu/\sqrt{S}$, the collinear approximation of the conventional parton model is recovered. In the collinear parton model, the hadronic cross section $d\sigma(p + p \to \mathcal{H} + X, S)$ and the relevant partonic cross section $d\hat{\sigma}(g + g \to \mathcal{H} + X, \hat{s})$ are related as

$$d\sigma^{\rm PM}(p + p \to \mathcal{H} + X, S) = \int dx_1 \, G(x_1, \mu^2) \int dx_2 \, G(x_2, \mu^2) d\hat{\sigma}(g + g \to \mathcal{H} + X, \hat{s}), \quad (6)$$

where $\hat{s} = x_1 x_2 S$ and $G(x, \mu^2)$ is the collinear gluon distribution function of the proton, which satisfies the DGLAP [3] evolution equation. The collinear and the unintegrated gluon distribution functions are formally related as

$$xG(x, \mu^2) = \int_0^{\mu^2} d|\mathbf{k}_T|^2 \, \Phi(x, |\mathbf{k}_T|^2, \mu^2), \quad (7)$$

so that the normalizations of Eqs. (5) and (6) agree.

III. NRQCD FORMALISM

In the framework of the NRQCD factorization approach [1], the cross section of heavy-quarkonium production via a partonic subprocess $a + b \to \mathcal{H} + X$ may be presented as a sum of terms in which the effects of long and short distances are factorized as

$$d\hat{\sigma}(a + b \to \mathcal{H} + X) = \sum_n d\hat{\sigma}(a + b \to Q\bar{Q}[n] + X)\langle \mathcal{O}^{\mathcal{H}}[n] \rangle, \quad (8)$$

where n denotes the set of color, spin, orbital and total angular momentum quantum numbers of the $Q\bar{Q}$ pair and the four-momentum of the latter is assumed to be equal to the one of the physical quarkonium state $\mathcal{H}$. The cross section $d\hat{\sigma}(a + b \to Q\bar{Q}[n] + X)$ can be calculated in perturbative QCD as an expansion in α_s using the non-relativistic approximation for the relative motion of the heavy quarks in the $Q\bar{Q}$ pair. The non-perturbative transition of the $Q\bar{Q}$ pair into $\mathcal{H}$ is described by the NMEs $\langle \mathcal{O}^{\mathcal{H}}[n] \rangle$, which can be extracted from experimental data.

To LO in v, we need to include the $c\bar{c}$ Fock states $n = {}^3S_1^{(1)}, {}^3S_1^{(8)}, {}^1S_0^{(8)}, {}^3P_J^{(8)}$ if $\mathcal{H} = J/\psi, \psi'$ and $n = {}^3P_J^{(1)}, {}^3S_1^{(8)}$ if $\mathcal{H} = \chi_{cJ}$, where $J = 0, 1, 2$. Their NMEs satisfy the multiplicity relations

$$\begin{aligned}
\langle \mathcal{O}^{\psi(nS)}[{}^3P_J^{(8)}] \rangle &= (2J + 1)\langle \mathcal{O}^{\psi(nS)}[{}^3P_0^{(8)}] \rangle, \\
\langle \mathcal{O}^{\chi_{cJ}}[{}^3P_J^{(1)}] \rangle &= (2J + 1)\langle \mathcal{O}^{\chi_{c0}}[{}^3P_0^{(1)}] \rangle, \\
\langle \mathcal{O}^{\chi_{cJ}}[{}^3S_1^{(8)}] \rangle &= (2J + 1)\langle \mathcal{O}^{\chi_{c0}}[{}^3S_1^{(8)}] \rangle,
\end{aligned} \quad (9)$$

which follow to LO in v from heavy-quark spin symmetry. For example, in the case of J/ψ production, the wave function of the physical orthocharmonium state can be presented as a superposition of the Fock states:

$$
\begin{aligned}
|J/\psi\rangle \;=\; & \mathcal{O}(v^0)|c\bar{c}[^3S_1^{(1)}]\rangle + \mathcal{O}(v^1)|c\bar{c}[^3P_J^{(8)}]g\rangle + \mathcal{O}(v^2)|c\bar{c}[^3S_1^{(1,8)}]gg\rangle \\
& + \mathcal{O}(v^2)|c\bar{c}[^1S_0^{(8)}]g\rangle + \cdots,
\end{aligned}
\tag{10}
$$

where we use usual spectroscopic notation for the angular-momentum quantum numbers of the $Q\bar{Q}$ pair and the index in parentheses $(1,8)$ denotes the color state, either color singlet or color octet. The color-singlet model (CSM) [16] only takes into account the first term in Eq. (10), which is of order v^0. In this case, the NME $\langle\mathcal{O}^{J/\psi}[^3S_1^{(1)}]\rangle$ is directly related to the J/ψ wave function at the origin $\Psi(0)$, which can be calculated in the framework of the quark potential model [17], as

$$
\langle\mathcal{O}^{J/\psi}[^3S_1^{(1)}]\rangle = 2N_c(2J+1)|\Psi(0)|^2,
\tag{11}
$$

where $N_c = 3$ and $J = 1$. Similarly, the color-singlet P-wave NME reads

$$
\langle\mathcal{O}^{\chi_{cJ}}[^3P_J^{(1)}]\rangle = 2N_c(2J+1)|\Psi'(0)|^2,
\tag{12}
$$

where $\Psi'(0)$ is the derivative of the χ_{cJ} wave function at the origin.

In the general case, the partonic cross section of quarkonium production receives from the $Q\bar{Q}$ Fock state $n = {}^{2S+1}L_J^{(1,8)}$ the contribution [1, 18]

$$
d\hat{\sigma}(a + b \to Q\bar{Q}[^{2S+1}L_J^{(1,8)}] \to \mathcal{H}) = d\hat{\sigma}(a + b \to Q\bar{Q}[^{2S+1}L_J^{(1,8)}])\frac{\langle\mathcal{O}^{\mathcal{H}}[^{2S+1}L_J^{(1,8)}]\rangle}{N_{\text{col}}N_{\text{pol}}},
\tag{13}
$$

where $N_{\text{col}} = 2N_c$ for the color-singlet state, $N_{\text{col}} = N_c^2 - 1$ for the color-octet state, and $N_{\text{pol}} = 2J + 1$. The partonic cross section of $Q\bar{Q}$ production is defined as

$$
d\hat{\sigma}(a + b \to Q\bar{Q}[^{2S+1}L_J^{(1,8)}]) = \frac{1}{I}\overline{|\mathcal{A}(a + b \to Q\bar{Q}[^{2S+1}L_J^{(1,8)}])|^2}d\Phi,
\tag{14}
$$

where I is the flux factor of the incoming particles, which is taken as in the collinear parton model [6] (for example, $I = 2x_1x_2S$ for process (4)), $\mathcal{A}(a + b \to Q\bar{Q}[^{2S+1}L_J^{(1,8)}])$ is the production amplitude, the bar indicates average (summation) over initial-state (final-state) spins and colors, and $d\Phi$ is the phase space volume of the outgoing particles. This convention implies that the cross section in the k_T-factorization approach is normalized approximately to the cross section for on-shell gluons when $\mathbf{k}_{1T} = \mathbf{k}_{2T} = \mathbf{0}$.

The production amplitude $\mathcal{A}(a + b \to Q\bar{Q}[^{2S+1}L_J^{(1,8)}])$ can be obtained from the one for an unspecified $Q\bar{Q}$ state, $\mathcal{A}(a+b \to Q\bar{Q})$, by the application of appropriate projectors. The projectors on the spin-zero and spin-one states read [19]:

$$\Pi_0 = \frac{1}{\sqrt{8m^3}} \left(\frac{\hat{p}}{2} - \hat{q} - m \right) \gamma_5 \left(\frac{\hat{p}}{2} + \hat{q} + m \right),$$

$$\Pi_1^\alpha = \frac{1}{\sqrt{8m^3}} \left(\frac{\hat{p}}{2} - \hat{q} - m \right) \gamma^\alpha \left(\frac{\hat{p}}{2} + \hat{q} + m \right), \tag{15}$$

respectively, where $\hat{p} = \gamma^\mu p_\mu$, p^μ is the four-momentum of the $Q\bar{Q}$ pair, q^μ is the four-momentum of the relative motion, $m = M/2$ is the mass of the quark Q, and M is the mass of the quarkonium state $\mathcal{H}$. In our numerical calculations, we use $m_c = 1.55$ GeV. The projection operators for the color-singlet and color-octet states read:

$$C_1 = \frac{\delta_{ij}}{\sqrt{N_c}},$$

$$C_8 = \sqrt{2} T_{ij}^a, \tag{16}$$

respectively, where T^a with $a = 1, \ldots, N_c^2 - 1$ are the generators of the color gauge group SU(3). To obtain the projection on a state with orbital-angular-momentum quantum number L, we need to take L times the derivative with respect to q and then put $q = 0$. For the processes discussed here, we have

$$\mathcal{A}(a + b \to Q\bar{Q}[^1S_0^{(1,8)}]) = \text{Tr}\left[C_{1,8} \Pi_0 \mathcal{A}(a + b \to Q\bar{Q}) \right]_{q=0},$$

$$\mathcal{A}(a + b \to Q\bar{Q}[^3S_1^{(1,8)}]) = \text{Tr}\left[C_{1,8} \Pi_1^\alpha \mathcal{A}(a + b \to Q\bar{Q}) \varepsilon_\alpha(p) \right]_{q=0},$$

$$\mathcal{A}(a + b \to Q\bar{Q}[^3P_J^{(1,8)}]) = \frac{d}{dq_\beta} \text{Tr}\left[C_{1,8} \Pi_1^\alpha \mathcal{A}(a + b \to Q\bar{Q}) \varepsilon_{\alpha\beta}(p) \right]_{q=0}, \tag{17}$$

where $\varepsilon_\alpha(p)$ is the polarization four-vector of a spin-one particle with four-momentum p^μ and mass $M = p^2$ and $\varepsilon_{\alpha\beta}(p)$ is its counterpart for a spin-two particle. For the $^3S_1$ state, the polarization sum reads

$$\sum_{J_z} \varepsilon_\alpha(p) \varepsilon_{\alpha'}^*(p) = \mathcal{P}_{\alpha\alpha'}(p) = -g_{\alpha\alpha'} + \frac{p_\alpha p_{\alpha'}}{M^2}. \tag{18}$$

For the ^3P_J states with $J = 0, 1, 2$, we have

$$\varepsilon_{\alpha\beta}^{(0)}(p) \varepsilon_{\alpha'\beta'}^{(0)*}(p) = \frac{1}{3} \mathcal{P}_{\alpha\beta}(p) \mathcal{P}_{\alpha'\beta'}(p),$$

$$\sum_{J_z} \varepsilon_{\alpha\beta}^{(1)}(p) \varepsilon_{\alpha'\beta'}^{(1)*}(p) = \frac{1}{2} \left[\mathcal{P}_{\alpha\alpha'}(p) \mathcal{P}_{\beta\beta'}(p) - \mathcal{P}_{\alpha\beta'}(p) \mathcal{P}_{\alpha'\beta}(p) \right],$$

$$\sum_{J_z} \varepsilon_{\alpha\beta}^{(2)}(p) \varepsilon_{\alpha'\beta'}^{(2)*}(p) = \frac{1}{2} \left[\mathcal{P}_{\alpha\alpha'}(p) \mathcal{P}_{\beta\beta'}(p) + \mathcal{P}_{\alpha\beta'}(p) \mathcal{P}_{\alpha'\beta}(p) \right] - \frac{1}{3} \mathcal{P}_{\alpha\beta} \mathcal{P}_{\alpha'\beta'}(p). \tag{19}$$

The subprocesses relevant for our analysis read: $R + R \rightarrow Q\bar{Q}$, $R + R \rightarrow Q\overline{Q} + g$, $R + \gamma \rightarrow Q\overline{Q}$, $R + \gamma \rightarrow Q\overline{Q} + g$, $R + e \rightarrow e + Q\overline{Q}$, and $R + e \rightarrow e + Q\overline{Q} + g$.

IV. CHARMONIUM PRODUCTION BY REGGEIZED GLUONS

In this section, we obtain the squared amplitudes for inclusive charmonium production via the fusion of two reggeized gluons or a reggeized gluon and a real or virtual photon in the framework of NRQCD. We work at LO in α_s and v and consider the following partonic subprocesses:

$$R + R \rightarrow \mathcal{H}[^3P_J^{(1)}, {}^3S_1^{(8)}, {}^1S_0^{(8)}, {}^3P_J^{(8)}], \tag{20}$$

$$R + R \rightarrow \mathcal{H}[^3S_1^{(1)}] + g, \tag{21}$$

$$R + \gamma \rightarrow \mathcal{H}[^3S_1^{(8)}, {}^1S_0^{(8)}, {}^3P_J^{(8)}], \tag{22}$$

$$R + \gamma \rightarrow \mathcal{H}[^3S_1^{(1)}] + g, \tag{23}$$

$$R + e \rightarrow e + \mathcal{H}[^3S_1^{(8)}, {}^1S_0^{(8)}, {}^3P_J^{(8)}], \tag{24}$$

$$R + e \rightarrow e + \mathcal{H}[^3S_1^{(1)}] + g. \tag{25}$$

Notice that, in the collinear parton model, subprocesses (20), (22), and (24) only contribute for $p_T \approx 0$. Therefore, to LO in the collinear parton model, we need to take into account the corresponding subprocesses with an additional hard gluon in the final state, for example $g + g \rightarrow \mathcal{H}[^3S_1^{(8)}] + g$. The amplitudes of these color-octet subprocesses, after replacing $g \rightarrow R$ in the initial state, are of next-to-leading order (NLO) in the k_T-factorization approach and suffer from infrared divergences, in contrast to the subprocesses (21) and (23) in the color-singlet channel. The analysis of NLO contributions to inclusive charmonium production by reggeized gluon-gluon fusion in the k_T-factorization approach is beyond the scope of this paper and needs a separate investigation.

The phenomenological procedure, adopted in Ref. [20], to regularize infrared divergences due to propagators getting on-shell with the help of some cut parameter, which is unknown a priori, is likely to be problematic. The analysis of NLO corrections in the k_T-factorization approach is currently an open issue, which has been consistently solved only in part, e.g. in Ref. [21], where NLO corrections to the subprocess $R + R \rightarrow g$ were studied.

According to the prescription of Ref. [6], the amplitude of $R + R \rightarrow c + \bar{c}(+g)$ is related

to the one of $g + g \to c + \bar{c}(+g)$ by

$$\mathcal{A}(R + R \to c + \bar{c}(+g)) = \varepsilon^\mu(k_1)\varepsilon^\nu(k_2)\mathcal{A}_{\mu\nu}(g + g \to c + \bar{c}(+g)), \tag{26}$$

where $\varepsilon^\mu(k_1)$ and $\varepsilon^\mu(k_2)$ are defined according to Eq. (1). Analogous relations hold for $R + \gamma \to c + \bar{c}(+g)$ and $R + e \to e + c + \bar{c}(+g)$. The amplitudes of the relevant QCD subprocesses $g + g \to c + \bar{c}(+g)$, $g + \gamma \to c + \bar{c}(+g)$, and $g + e \to e + c + \bar{c}(+g)$ are evaluated using the conventional Feynman rules of QCD.

We now present and discuss our results for the squared amplitudes of subprocesses (20) and (21), contributing to hadroproduction. In the case of the $2 \to 1$ subprocesses (20), we obtain

$$\overline{|\mathcal{A}(R + R \to \mathcal{H}[^3P_0^{(1)}])|^2} = \frac{8}{3}\pi^2\alpha_s^2\frac{\langle\mathcal{O}^\mathcal{H}[^3P_0^{(1)}]\rangle}{M^5}F^{[^3P_0]}(t_1, t_2, \varphi),$$

$$\overline{|\mathcal{A}(R + R \to \mathcal{H}[^3P_1^{(1)}])|^2} = \frac{16}{3}\pi^2\alpha_s^2\frac{\langle\mathcal{O}^\mathcal{H}[^3P_1^{(1)}]\rangle}{M^5}F^{[^3P_1]}(t_1, t_2, \varphi),$$

$$\overline{|\mathcal{A}(R + R \to \mathcal{H}[^3P_2^{(1)}])|^2} = \frac{32}{45}\pi^2\alpha_s^2\frac{\langle\mathcal{O}^\mathcal{H}[^3P_2^{(1)}]\rangle}{M^5}F^{[^3P_2]}(t_1, t_2, \varphi),$$

$$\overline{|\mathcal{A}(R + R \to \mathcal{H}[^3S_1^{(8)}])|^2} = \frac{1}{2}\pi^2\alpha_s^2\frac{\langle\mathcal{O}^\mathcal{H}[^3S_1^{(8)}]\rangle}{M^3}F^{[^3S_1]}(t_1, t_2, \varphi),$$

$$\overline{|\mathcal{A}(R + R \to \mathcal{H}[^1S_0^{(8)}])|^2} = \frac{5}{12}\pi^2\alpha_s^2\frac{\langle\mathcal{O}^\mathcal{H}[^1S_0^{(8)}]\rangle}{M^3}F^{[^1S_0]}(t_1, t_2, \varphi),$$

$$\overline{|\mathcal{A}(R + R \to \mathcal{H}[^3P_0^{(8)}])|^2} = 5\pi^2\alpha_s^2\frac{\langle\mathcal{O}^\mathcal{H}[^3P_0^{(8)}]\rangle}{M^5}F^{[^3P_0]}(t_1, t_2, \varphi),$$

$$\overline{|\mathcal{A}(R + R \to \mathcal{H}[^3P_1^{(8)}])|^2} = 10\pi^2\alpha_s^2\frac{\langle\mathcal{O}^\mathcal{H}[^3P_1^{(8)}]\rangle}{M^5}F^{[^3P_1]}(t_1, t_2, \varphi),$$

$$\overline{|\mathcal{A}(R + R \to \mathcal{H}[^3P_2^{(8)}])|^2} = \frac{4}{3}\pi^2\alpha_s^2\frac{\langle\mathcal{O}^\mathcal{H}[^3P_2^{(8)}]\rangle}{M^5}F^{[^3P_2]}(t_1, t_2, \varphi), \tag{27}$$

where

$$F^{[^3S_1]}(t_1, t_2, \varphi) = \frac{(M^2 + |\mathbf{p}_T|^2)\left[(t_1 + t_2)^2 + M^2\left(t_1 + t_2 - 2\sqrt{t_1 t_2}\cos\varphi\right)\right]}{(M^2 + t_1 + t_2)^2},$$

$$F^{[^1S_0]}(t_1, t_2, \varphi) = 2\frac{M^2}{(M^2 + t_1 + t_2)^2}\left(M^2 + |\mathbf{p}_T|^2\right)^2\sin^2\varphi,$$

$$F^{[^3P_0]}(t_1, t_2, \varphi) = \frac{2}{9}\frac{M^2\left(M^2 + |\mathbf{p}_T|^2\right)^2\left[(3M^2 + t_1 + t_2)\cos\varphi + 2\sqrt{t_1 t_2}\right]^2}{(M^2 + t_1 + t_2)^4},$$

$$F^{[^3P_1]}(t_1, t_2, \varphi) = \frac{2}{9}\frac{M^2\left(M^2 + |\mathbf{p}_T|^2\right)^2\left[(t_1 + t_2)^2\sin^2\varphi + M^2\left(t_1 + t_2 - 2\sqrt{t_1 t_2}\cos\varphi\right)\right]}{(M^2 + t_1 + t_2)^4},$$

$$F^{[^3P_2]}(t_1, t_2, \varphi) = \frac{1}{3}\frac{M^2}{(M^2 + t_1 + t_2)^4}\left(M^2 + |\mathbf{p}_T|^2\right)^2\left\{3M^4 + 3M^2(t_1 + t_2) + 4t_1 t_2\right.$$

9

$$+ (t_1 + t_2)^2 \cos^2 \varphi + 2\sqrt{t_1 t_2} \left[3M^2 + 2(t_1 + t_2) \right] \cos \varphi \Big\}. \tag{28}$$

Here $\mathbf{p}_T = \mathbf{k}_{1T} + \mathbf{k}_{2T}$, $t_{1,2} = |\mathbf{k}_{1,2T}|^2$, and $\varphi = \varphi_1 - \varphi_2$ is the angle enclosed between $\mathbf{k}_{1T}$ and $\mathbf{k}_{2T}$, so that

$$|\mathbf{p}_T|^2 = t_1 + t_2 + 2\sqrt{t_1 t_2} \cos \varphi. \tag{29}$$

It is interesting to consider the contribution of the diagram involving a three-gluon vertex separately. It is equal to

$$\overline{|\mathcal{A}_3(R + R \to \mathcal{H}[^3S_1^{(8)}])|^2} = \pi^2 \alpha_s^2 \frac{\langle \mathcal{O}^{\mathcal{H}}[^3S_1^{(8)}] \rangle}{2M^3} (M^2 \cos^2 \varphi + |\mathbf{p}_T|^2). \tag{30}$$

For $|\mathbf{p}_T|^2 \gg M^2$, one has

$$\overline{|\mathcal{A}_3(R + R \to \mathcal{H}[^3S_1^{(8)}])|^2} \approx \pi^2 \alpha_s^2 \frac{\langle \mathcal{O}^{\mathcal{H}}[^3S_1^{(8)}] \rangle}{2M^3} |\mathbf{p}_T|^2, \tag{31}$$

which makes up the bulk of the contribution and can be interpreted as being due to the fragmentation production of the $\mathcal{H}$ meson. In fact, the right-hand side of Eq. (31) can be written in the factorized form

$$\overline{|\mathcal{A}_3(R + R \to \mathcal{H}[^3S_1^{(8)}])|^2} \approx \overline{|\mathcal{A}(R + R \to g)|^2} P(g \to \mathcal{H}[^3S_1^{(8)}]), \tag{32}$$

where

$$\overline{|\mathcal{A}(R + R \to g)|^2} = \frac{3}{2} \pi \alpha_s |\mathbf{p}_T|^2 \tag{33}$$

refers to real-gluon production by reggeized-gluon fusion [10] and

$$P(g \to \mathcal{H}[^3S_1^{(8)}]) = \pi \alpha_s \frac{\langle \mathcal{O}^{\mathcal{H}}[^3S_1^{(8)}] \rangle}{3M^3} \tag{34}$$

is the probability for the fragmentation of a gluon to a $\mathcal{H}$ meson, which may be gleaned from the result for the corresponding fragmentation function at the starting scale μ_0 [22],

$$D_{g \to \mathcal{H}[^3S_1^{(8)}]}(z, \mu_0) = \pi \alpha_s \frac{\langle \mathcal{O}^{\mathcal{H}}[^3S_1^{(8)}] \rangle}{3M^3} \delta(1 - z). \tag{35}$$

The counterparts of Eq. (27) in the collinear parton model of QCD emerge through the operation

$$\overline{|\mathcal{A}(g + g \to \mathcal{H}[^{2S+1}L_J^{(1,8)}])|^2} = \lim_{t_1, t_2 \to 0} \int_0^{2\pi} \frac{d\varphi_1}{2\pi} \int_0^{2\pi} \frac{d\varphi_2}{2\pi} \overline{|\mathcal{A}(R + R \to \mathcal{H}[^{2S+1}L_J^{(1,8)}])|^2}. \tag{36}$$

10

In this way, we recover the well-known results [23]:

$$\overline{|\mathcal{A}(g+g \to \mathcal{H}[^3P_0^{(1)}]|^2} = \frac{8}{3}\pi^2\alpha_s^2\frac{\langle\mathcal{O}^{\mathcal{H}}[^3P_0^{(1)}]\rangle}{M^3},$$

$$\overline{|\mathcal{A}(g+g \to \mathcal{H}[^3P_1^{(1)}]|^2} = 0,$$

$$\overline{|\mathcal{A}(g+g \to \mathcal{H}[^3P_2^{(1)}]|^2} = \frac{32}{45}\pi^2\alpha_s^2\frac{\langle\mathcal{O}^{\mathcal{H}}[^3P_2^{(1)}]\rangle}{M^3},$$

$$\overline{|\mathcal{A}(g+g \to \mathcal{H}[^3S_1^{(8)}]|^2} = 0,$$

$$\overline{|\mathcal{A}(g+g \to \mathcal{H}[^1S_0^{(8)}]|^2} = \frac{5}{12}\pi^2\alpha_s^2\frac{\langle\mathcal{O}^{\mathcal{H}}[^1S_0^{(8)}]\rangle}{M},$$

$$\overline{|\mathcal{A}(g+g \to \mathcal{H}[^3P_0^{(8)}]|^2} = 5\pi^2\alpha_s^2\frac{\langle\mathcal{O}^{\mathcal{H}}[^3P_0^{(8)}]\rangle}{M^3},$$

$$\overline{|\mathcal{A}(g+g \to \mathcal{H}[^3P_1^{(8)}]|^2} = 0,$$

$$\overline{|\mathcal{A}(g+g \to \mathcal{H}[^3P_2^{(8)}]|^2} = \frac{4}{3}\pi^2\alpha_s^2\frac{\langle\mathcal{O}^{\mathcal{H}}[^3P_2^{(8)}]\rangle}{M^3}. \tag{37}$$

In the case of the $2 \to 2$ subprocess (21), we find

$$\overline{|\mathcal{A}(R+R \to \mathcal{H}[^3S_1^{(1)}]+g|^2} = \pi^3\alpha_s^3\frac{\langle\mathcal{O}^{\mathcal{H}}[^3S_1^{(1)}]\rangle}{M^3}$$

$$\times \frac{-320M^4}{81(M^2-\hat{s})^2(M^2+t_1-\hat{t})^2(M^2+t_2-\hat{u})^2}(4t_1t_2M^2(t_1+t_2+M^2)^2\cos^4(\varphi_1-\varphi_2)$$

$$-2\sqrt{t_1t_2}(t_1+t_2+M^2)\cos^3(\varphi_1-\varphi_2)(-t_2^2M^2-3M^6+t_2^2\hat{t}+3M^4\hat{t}+t_2M^2\hat{u}+3M^4\hat{u}$$

$$+t_2\hat{t}\hat{u}-M^2\hat{t}\hat{u}+t_1^2(t_2-M^2+\hat{u})+t_1(t_2^2+\hat{t}(M^2+\hat{u})+t_2(5M^2+\hat{t}+\hat{u}))$$

$$-2\sqrt{t_2}|\mathbf{p}_T|(t_1^2-(t_2-M^2)(M^2-\hat{t})+t_1(t_2+2M^2+\hat{t}))\cos\varphi_2)$$

$$-(-M^2+\hat{t}+\hat{u})^2(t_2^2M^2+t_2M^4+t_1^2(t_2+M^2)+t_2\hat{t}^2+M^2\hat{t}^2+M^2\hat{u}^2$$

$$+t_1(t_2^2+M^4+\hat{u}^2+2t_2(4M^2+\hat{t}+\hat{u}))-2\sqrt{t_2}|\mathbf{p}_T|(t_1^2+(t_2+M^2)(M^2-\hat{t})$$

$$+t_1(t_2+8M^2+\hat{t}+2\hat{u}))\cos\varphi_2+(t_1^2+(t_2+M^2)^2+2t_1(t_2+5M^2))|\mathbf{p}_T|^2\cos^2\varphi_2)$$

$$+\cos^2(\varphi_1-\varphi_2)(t_2^3M^4-2t_2^2M^6+5t_2M^8-2t_2^3M^2\hat{t}+4t_2^2M^4\hat{t}-10t_2M^6\hat{t}+t_2^3\hat{t}^2$$

$$-2t_2^2M^2\hat{t}^2+5t_2M^4\hat{t}^2-t_2^3M^2\hat{u}-7t_2M^6\hat{u}+t_2^3\hat{t}\hat{u}-t_2^2M^2\hat{t}\hat{u}+11t_2M^4\hat{t}\hat{u}-3M^6\hat{t}\hat{u}$$

$$+t_2^2\hat{t}^2\hat{u}-4t_2M^2\hat{t}^2\hat{u}+3M^4\hat{t}^2\hat{u}+2t_2M^4\hat{u}^2+t_2^2\hat{t}\hat{u}^2+3M^4\hat{t}\hat{u}^2-2M^2\hat{t}^2\hat{u}^2$$

$$+t_1^3(-4t_2^2+(M^2-\hat{u})(M^2-\hat{t}-\hat{u})+t_2(-5M^2+\hat{t}+\hat{u}))+t_1^2(-4t_2^3-2M^6+4M^4\hat{u}$$

$$+\hat{t}\hat{u}(\hat{t}+\hat{u})-2t_2^2(12M^2+\hat{t}+\hat{u})-M^2\hat{u}(\hat{t}+2\hat{u})+t_2(-25M^4+\hat{t}^2+7\hat{t}\hat{u}+2\hat{u}^2$$

$$+M^2(8\hat{t}+15\hat{u})))+t_1(5M^8-4M^2\hat{t}\hat{u}^2+t_2^3(-5M^2+\hat{t}+\hat{u})-M^6(7\hat{t}+10\hat{u})$$

$$+M^4(2\hat{t}^2+11\hat{t}\hat{u}+5\hat{u}^2)+t_2^2(-25M^4+2\hat{t}^2+7\hat{t}\hat{u}+\hat{u}^2+M^2(15\hat{t}+8\hat{u}))$$

$$+t_2(-11M^6+15M^4(\hat{t}+\hat{u})+6\hat{t}\hat{u}(\hat{t}+\hat{u})-2M^2(4\hat{t}^2+3\hat{t}\hat{u}+4\hat{u}^2)))$$

11

$$+ 2\sqrt{t_2}|\mathbf{p}_T|(t_1^4 + t_1^3(3t_2 + 11M^2 + \hat{s} + \hat{t}) + t_1^2(3t_2^2 + 7M^4 + \hat{s}\hat{t} + t_2(33M^2 - 2\hat{s} + 3\hat{t})$$

$$+ M^2(11\hat{s} + 4\hat{t})) + t_1(t_2^3 - 3M^6 - 4M^2\hat{t}^2 + 7M^4(\hat{s} + \hat{t}) + t_2^2(5M^2 + \hat{s} + 3\hat{t})$$

$$+ t_2(27M^4 + 2M^2(\hat{s} - 10\hat{t}) + 6\hat{s}\hat{t})) - (M^2 - \hat{t})(t_2^3 - t_2M^4 + t_2^2\hat{s}$$

$$+ M^2(-4\hat{t}(\hat{s} + \hat{t}) + M^2(3\hat{s} + 4\hat{t})))) \cos\varphi_2 - 4t_2|\mathbf{p}_T|^2(t_1^3 + 2t_1^2(t_2 + 2M^2) + 2(M^3 - M\hat{t})^2$$

$$+ t_1(t_2^2 + 2t_2M^2 + 5M^4 - 4M^2\hat{t})) \cos^2\varphi_2 - |\mathbf{p}_T|^2\cos^2\varphi_1(2t_1^3t_2 + 4t_1^2t_2^2 + 2t_1t_2^3$$

$$+ 4t_1^2t_2M^2 + 8t_1t_2^2M^2 + t_1^2M^4 + 12t_1t_2M^4 + t_2^2M^4 + 6t_1M^6 + 10t_2M^6 + M^8$$

$$+ 4M^6|\mathbf{p}_T|^2 - 2t_1^2M^2\hat{t} - 4t_1t_2M^2\hat{t} - 2t_2^2M^2\hat{t} - 4t_1M^4\hat{t} - 20t_2M^4\hat{t} - 2M^6\hat{t}$$

$$- 8M^4|\mathbf{p}_T|^2\hat{t} + t_1^2\hat{t}^2 + 2t_1t_2\hat{t}^2 + t_2^2\hat{t}^2 + 2t_1M^2\hat{t}^2 + 10t_2M^2\hat{t}^2 + M^4\hat{t}^2 + 4M^2|\mathbf{p}_T|^2\hat{t}^2$$

$$- 2t_1^2M^2\hat{u} - 12t_1t_2M^2\hat{u} - 2t_2^2M^2\hat{u} - 12t_1M^4\hat{u} - 20t_2M^4\hat{u} - 2M^6\hat{u} - 8M^4|\mathbf{p}_T|^2\hat{u}$$

$$+ 2t_1^2\hat{t}\hat{u} + 4t_1t_2\hat{t}\hat{u} + 2t_2^2\hat{t}\hat{u} + 4t_1M^2\hat{t}\hat{u} + 20t_2M^2\hat{t}\hat{u} + 2M^4\hat{t}\hat{u} + 8M^2|\mathbf{p}_T|^2\hat{t}\hat{u} + t_1^2\hat{u}^2$$

$$+ 2t_1t_2\hat{u}^2 + t_2^2\hat{u}^2 + 6t_1M^2\hat{u}^2 + 10t_2M^2\hat{u}^2 + M^4\hat{u}^2 + 4M^2|\mathbf{p}_T|^2\hat{u}^2$$

$$- 8\sqrt{t_1}M^2|\mathbf{p}_T|(t_2 + M^2 - \hat{u})(M^2 - \hat{t} - \hat{u})\Big(\cos\varphi_1 + \cos(\varphi_1 - 2\varphi_2)\Big)$$

$$+ 4\sqrt{t_1t_2}\cos(\varphi_1 - \varphi_2)\Big(M^2 - \hat{t} - \hat{u}\Big)\Big((t_1 + t_2)^2 + M^2(5M^2 + 2t_1 + 6t_2 - 4\hat{u})\Big)$$

$$+ 2t_1\cos(2(\varphi_1 - \varphi_2))\Big(t_2\big((t_1 + t_2)^2 + M^2(2t_1 + 4t_2 + 5M^2 - 4\hat{u})\big) + 2M^2\big(M^2 - \hat{u}\big)^2\Big)$$

$$- 16M^2|\mathbf{p}_T|\sqrt{t_2}\cos\varphi_2\Big(M^2 - \hat{t} - \hat{u}\Big)^2 + 4M^2|\mathbf{p}_T|^2\cos(2\varphi_2)\Big(M^2(M^2 - 2\hat{t} - 2\hat{u}) + (\hat{t} + \hat{u})^2\Big)$$

$$- 2\sqrt{t_1}(M^2 - \hat{t} - \hat{u})\cos(\varphi_1 - \varphi_2)(-2|\mathbf{p}_T|(2t_1^2t_2 - M^6 + 2t_2^2(M^2 - \hat{t}) + M^4\hat{t} + M^4\hat{u} - 2M^2\hat{t}\hat{u}$$

$$+ t_2(8M^4 - 7M^2\hat{t} - \hat{t}(\hat{t} + \hat{u})) + t_1(2t_2^2 + M^2(3M^2 - \hat{t} - 3\hat{u}) + t_2(11M^2 + \hat{t} + 3\hat{u}))) \cos\varphi_2$$

$$+ \sqrt{t_2}(2t_2^2M^2 + 7t_2M^4 - M^6 + t_2^2|\mathbf{p}_T|^2 + 2t_2M^2|\mathbf{p}_T|^2 + 5M^4|\mathbf{p}_T|^2$$

$$+ t_1^2(2t_2 + 2M^2 + |\mathbf{p}_T|^2) - 4t_2M^2\hat{t} - 4M^2|\mathbf{p}_T|^2\hat{t} + t_2\hat{t}^2 + 3M^2\hat{t}^2 - t_2M^2\hat{u} - t_2\hat{t}\hat{u}$$

$$- M^2\hat{t}\hat{u} - \hat{t}^2\hat{u} + 3M^2\hat{u}^2 - \hat{t}\hat{u}^2 + t_1(2t_2^2 + 7M^4 + M^2(6|\mathbf{p}_T|^2 - \hat{t} - 4\hat{u}) + \hat{u}(-\hat{t} + \hat{u})$$

$$+ t_2(13M^2 + 2|\mathbf{p}_T|^2 + 3(\hat{t} + \hat{u}))) + |\mathbf{p}_T|^2(t_1^2 + t_2^2 + 2t_2M^2 + 5M^4 + 2t_1(t_2 + 3M^2)$$

$$- 4M^2\hat{t})\cos(2\varphi_2))) + 2|\mathbf{p}_T|\cos\varphi_1(2t_1\sqrt{t_2}(t_1 + t_2 + M^2)(t_2^2 + M^4 - M^2\hat{u}$$

$$+ t_1(t_2 - M^2 + \hat{u}) + t_2(2M^2 + \hat{u}))\cos^3(\varphi_1 - \varphi_2) + \sqrt{t_1}\cos^2(\varphi_1 - \varphi_2)(t_2^4 + 11t_2^3M^2 + 7t_2^2M^4$$

$$- 3t_2M^6 + t_2^3\hat{s} + 11t_2^2M^2\hat{s} + 7t_2M^4\hat{s} - 3M^6\hat{s} + t_2^3\hat{u} + 4t_2^2M^2\hat{u} + 7t_2M^4\hat{u} - 4M^6\hat{u}$$

$$+ t_2^2\hat{s}\hat{u} + 7M^4\hat{s}\hat{u} - 4t_2M^2\hat{u}^2 + 8M^4\hat{u}^2 - 4M^2\hat{s}\hat{u}^2 - 4M^2\hat{u}^3 + t_1^3(t_2 - M^2 + \hat{u})$$

$$+ t_1^2(3t_2^2 + \hat{s}(-M^2 + \hat{u}) + t_2(5M^2 + \hat{s} + 3\hat{u})) + t_1(3t_2^3 + M^6 - M^4\hat{u}$$

$$+ t_2^2(33M^2 - 2\hat{s} + 3\hat{u}) + t_2(27M^4 + 2M^2(\hat{s} - 10\hat{u}) + 6\hat{s}\hat{u})) + 2\sqrt{t_2}|\mathbf{p}_T|(-5M^6 + 5M^4\hat{t}$$

$$- 4t_2(M^4 - M^2\hat{t}) + t_1^2(M^2 - \hat{t} - \hat{u}) + t_2^2(M^2 - \hat{t} - \hat{u}) + 5M^4\hat{u} - 2t_1(2M^2(M^2 - \hat{u})$$

$$
\begin{aligned}
&+ t_2(M^2 + \hat{t} + \hat{u}))) \cos\varphi_2) + \sqrt{t_1}(-M^2 + \hat{t} + \hat{u})^2(t_1 t_2 + t_2^2 + t_1 M^2 + 8t_2 M^2 + M^4 \\
&+ 4M^2|\mathbf{p}_T|^2 + 2t_2\hat{t} - t_1\hat{u} + t_2\hat{u} - M^2\hat{u} - 2\sqrt{t_2}|\mathbf{p}_T|(7M^2 + \hat{t} + \hat{u})\cos\varphi_2 + 4M^2|\mathbf{p}_T|^2\cos(2\varphi_2)) \\
&- (M^2 - \hat{t} - \hat{u})\cos(\varphi_1 - \varphi_2)(-(|\mathbf{p}_T|(3M^6 - 3M^4\hat{t} - 12t_2(M^4 - M^2\hat{t}) + t_1^2(M^2 - \hat{t} - \hat{u}) \\
&+ t_2^2(M^2 - \hat{t} - \hat{u}) - 3M^4\hat{u} + 4M^2\hat{t}\hat{u} - 2t_1(6M^2(M^2 - \hat{u}) + t_2(11M^2 + 3(\hat{t} + \hat{u}))))\cos\varphi_2) \\
&- 2\sqrt{t_2}(2t_1^2(t_2 + M^2 - \hat{u}) - M^2(M^4 + 2\hat{t}(|\mathbf{p}_T|^2 + \hat{u}) - M^2(2|\mathbf{p}_T|^2 + \hat{t} + \hat{u}) \\
&+ t_2(-3M^2 + 3\hat{t} + \hat{u})) + t_1(2t_2^2 + 8M^4 + M^2(2|\mathbf{p}_T|^2 - 7\hat{u}) - \hat{u}(\hat{t} + \hat{u}) \\
&+ t_2(11M^2 + 3\hat{t} + \hat{u})) + 2M^2|\mathbf{p}_T|^2(t_1 + M^2 - \hat{t})\cos(2\varphi_2)))))),
\end{aligned} \tag{38}
$$

where $\hat{s} = (k_1 + k_2)^2$, $\hat{t} = (k_1 - p)^2$, and $\hat{u} = (k_2 - p)^2$ are the standard Mandelstam variables. With the aid of Eq. (36), we recover from Eq. (38) the well-known collinear-parton-model result [23],

$$
\begin{aligned}
\overline{|\mathcal{A}(g + g \to \mathcal{H}[^3S_1^{(1)}] + g|^2} &= \pi^3\alpha_s^3\frac{\langle\mathcal{O}^{\mathcal{H}}[^3S_1^{(1)}]\rangle}{M^3}\frac{320M^4}{81(M^2 - \hat{t})^2(M^2 - \hat{u})^2(\hat{t} + \hat{u})^2} \\
&\times (M^4\hat{t}^2 - 2M^2\hat{t}^3 + \hat{t}^4 + M^4\hat{t}\hat{u} - 3M^2\hat{t}^2\hat{u} + 2\hat{t}^3\hat{u} + M^4\hat{u}^2 \\
&- 3M^2\hat{t}\hat{u}^2 + 3\hat{t}^2\hat{u}^2 - 2M^2\hat{u}^3 + 2\hat{t}\hat{u}^3 + \hat{u}^4).
\end{aligned} \tag{39}
$$

We now turn to subprocesses (22) and (23), with one real photon in the initial state. For the $2 \to 1$ subprocesses (22), which are pure color-octet processes, we find

$$
\begin{aligned}
\overline{|\mathcal{A}(R + \gamma \to \mathcal{H}[^3S_1^{(8)}]|^2} &= 0, \\
\overline{|\mathcal{A}(R + \gamma \to \mathcal{H}[^1S_0^{(8)}]|^2} &= 8\pi^2\alpha\alpha_s e_Q^2\frac{\langle\mathcal{O}^{\mathcal{H}}[^1S_0^{(8)}]\rangle}{M}, \\
\overline{|\mathcal{A}(R + \gamma \to \mathcal{H}[^3P_0^{(8)}]|^2} &= \frac{32}{3}\pi^2\alpha\alpha_s e_Q^2\frac{\langle\mathcal{O}^{\mathcal{H}}[^3P_0^{(8)}]\rangle}{M^3}\frac{(3M^2 + t_1)^2}{(M^2 + t_1)^2}, \\
\overline{|\mathcal{A}(R + \gamma \to \mathcal{H}[^3P_1^{(8)}]|^2} &= \frac{64}{3}\pi^2\alpha\alpha_s e_Q^2\frac{\langle\mathcal{O}^{\mathcal{H}}[^3P_1^{(8)}]\rangle}{M^3}\frac{t_1(2M^2 + t_1)}{(M^2 + t_1)^2}, \\
\overline{|\mathcal{A}(R + \gamma \to \mathcal{H}[^3P_2^{(8)}]|^2} &= \frac{64}{15}\pi^2\alpha\alpha_s e_Q^2\frac{\langle\mathcal{O}^{\mathcal{H}}[^3P_2^{(8)}]\rangle}{M^3}\frac{6M^4 + 6M^2t_1 + t_1^2}{(M^2 + t_1)^2},
\end{aligned} \tag{40}
$$

where e_Q is electric charge of the heavy quark Q. Application of Eq. (36) to Eq. (40) yields the well-known results of the collinear parton model [24],

$$
\begin{aligned}
\overline{|\mathcal{A}(g + \gamma \to \mathcal{H}[^3S_1^{(8)}]|^2} &= 0, \\
\overline{|\mathcal{A}(g + \gamma \to \mathcal{H}[^1S_0^{(8)}]|^2} &= 8\pi^2\alpha\alpha_s e_Q^2\frac{\langle\mathcal{O}^{\mathcal{H}}[^1S_0^{(8)}]\rangle}{M}, \\
\overline{|\mathcal{A}(g + \gamma \to \mathcal{H}[^3P_0^{(8)}]|^2} &= 96\pi^2\alpha\alpha_s e_Q^2\frac{\langle\mathcal{O}^{\mathcal{H}}[^3P_0^{(8)}]\rangle}{M^3},
\end{aligned}
$$

$$\overline{|\mathcal{A}(g+\gamma \to \mathcal{H}[^3P_1^{(8)}]|^2} = 0,$$

$$\overline{|\mathcal{A}(g+\gamma \to \mathcal{H}[^3P_2^{(8)}]|^2} = \frac{128}{5}\pi^2\alpha\alpha_s e_Q^2 \frac{\langle \mathcal{O}^{\mathcal{H}}[^3P_2^{(8)}]\rangle}{M^3}. \tag{41}$$

For the $2 \to 2$ subprocess (23), which is a color-singlet process, we find

$$\overline{|\mathcal{A}(R+\gamma \to \mathcal{H}[^3S_1^{(1)}]+g|^2} = \pi^3\alpha\alpha_s^2 e_Q^2 \frac{\langle \mathcal{O}^{\mathcal{H}}[^3S_1^{(1)}]\rangle}{M^3} \frac{2048M^2}{27(M^2-\hat{s})^2(M^2-\hat{u})^2(t_1+M^2-\hat{t})^2}$$

$$\times \left(t_1^4 M^2 + M^2(\hat{s}^2 + \hat{s}\hat{u} + \hat{u}^2 - M^2(\hat{s}+\hat{u}))^2 + t_1^3(M^2(5\hat{s}+3\hat{u}) - 7M^4 - \hat{s}\hat{u})\right.$$

$$+ t_1^2(\hat{s}\hat{u}(\hat{u}-\hat{s}) + M^4(3\hat{u}-11\hat{s}) + M^2(7\hat{s}^2 + 2\hat{s}\hat{u} - 3\hat{u}^2)) + t_1\hat{s}(\hat{s}\hat{u}^2 + M^4(\hat{u}-6\hat{s})$$

$$+ M^2(4\hat{s}^2 + \hat{s}\hat{u} - \hat{u}^2)) - 2\sqrt{t_1}|\mathbf{p}_T|(t_1^3 M^2 + t_1^2(-7M^4 - \hat{s}\hat{u} + M^2(3\hat{s}+4\hat{u}))$$

$$+ t_1(M^4(-7\hat{s}+2\hat{u}) - \hat{s}^2\hat{u} + M^2(2\hat{s}^2 + \hat{s}\hat{u} - 2\hat{u}^2)) - M^2(2M^4(\hat{s}+\hat{u}) - 2M^2\hat{u}(3\hat{s}+2\hat{u})$$

$$+ \hat{u}(3\hat{s}^2 + 4\hat{s}\hat{u} + 2\hat{u}^2)))\cos\varphi - 2M^2|\mathbf{p}_T|^2(t_1^3 + M^2\hat{s}^2 + t_1^2(M^2+2\hat{s})$$

$$\left. + t_1(2M^2\hat{s} + \hat{s}^2 - 2\hat{t}^2))\cos^2\varphi\right), \tag{42}$$

where k_2^μ now represents the photon four-momentum and $\varphi_2 = 0$. Equation (42) agrees with the corresponding result in Ref. [25], but has a more compact form. By means of Eq. (36), Eq. (42) collapses to the well-known collinear-parton model result [26],

$$\overline{|\mathcal{A}(g+\gamma \to \mathcal{H}[^3S_1^{(1)}]+g|^2} = \pi^3\alpha\alpha_s^2 e_Q^2 \frac{\langle \mathcal{O}^{\mathcal{H}}[^3S_1^{(1)}]\rangle}{M^3} \frac{2048M^4}{27(M^2-\hat{t})^2(M^2-\hat{u})^2(\hat{t}+\hat{u})^2}$$

$$\times (M^4\hat{t}^2 - 2M^2\hat{t}^3 + \hat{t}^4 + M^4\hat{t}\hat{u} - 3M^2\hat{t}^2\hat{u} + 2\hat{t}^3\hat{u} + M^4\hat{u}^2$$

$$- 3M^2\hat{t}\hat{u}^2 + 3\hat{t}^2\hat{u}^2 - 2M^2\hat{u}^3 + 2\hat{t}\hat{u}^3 + \hat{u}^4). \tag{43}$$

Finally, we turn to subprocesses (24) and (25), through which electroproduction proceeds at LO. As for the $2 \to 2$ subprocesses (24), which are all color-octet processes, we have

$$\overline{|\mathcal{A}(R+e \to e + \mathcal{H}[^3S_1^{(8)}]|^2} = 0,$$

$$\overline{|\mathcal{A}(R+e \to e + \mathcal{H}[^1S_0^{(8)}]|^2} = 64\pi^3\alpha^2\alpha_s e_Q^2 \frac{\langle \mathcal{O}^{\mathcal{H}}[^1S_0^{(8)}]\rangle}{M^3} \frac{1}{y_2^2 Q^2(M^2+Q^2+t_1)^2}$$

$$\times \left((2+(y_2-2)y_2)\left((M^2+t_1)^2 + Q^4 + 2Q^2M^2 - 2Q^2t_1y_2\right) + 4Q^2t_1\right.$$

$$+ 4Q\sqrt{t_1(1-y_2)}(M^2+Q^2+t_1)(y_2-2)y_2\cos(\varphi_1-\varphi_2)$$

$$\left.+ 2(y_2-1)\left(Q^4 + (M^2+t_1)^2 + Q^2(2M^2+2t_1-t_1y_2^2)\right)\cos(2(\varphi_1-\varphi_2))\right)M^2,$$

$$\overline{|\mathcal{A}(R+e \to e + \mathcal{H}[^3P_0^{(8)}]|^2} = \frac{256}{3}\pi^3\alpha^2\alpha_s e_Q^2 \frac{\langle \mathcal{O}^{\mathcal{H}}[^3P_0^{(8)}]\rangle}{M^5} \frac{1}{y_2^2 Q^2(M^2+Q^2+t_1)^4}$$

$$\times \left((2+(y_2-2)y_2)\left(9M^8 + 24M^6(Q^2+t_1) + 22M^4Q^4 + 22M^4t_1^2 + (Q^2+t_1)^2(Q^4+t_1^2)\right.\right.$$

14

$$+ 8M^2(Q^2 + t_1)(Q^4 + t_1^2)\Big) + 2M^4Q^2t_1(52 + y_2((43 - 9y_2)y_2 - 64))$$

$$+ 2Q^2t_1(Q^2 + t_1)^2(10 - y_2(14 + (y_2 - 6)y_2))$$

$$+ 4M^2Q^2t_1(Q^2 + t_1)(16 - 3y_2(8 + (y_2 - 5)y_2))$$

$$+ 4Q\sqrt{t_1(1 - y_2)}(M^2 + Q^2 + t_1)(Q^4(4 + (y_2 - 2)y_2) + 2Q^2(t_1(4 + (y_2 - 6)y_2)$$

$$+ M^2(8 + y_2(-4 + 3y_2))) + (3M^2 + t_1)(t_1(4 + (y_2 - 2)y_2)$$

$$+ M^2(4 + y_2(3y_2 - 2)))) \cos(\varphi_1 - \varphi_2) - 2(3M^2 + Q^2 + t_1)(y_2 - 1)$$

$$\times (3M^6 + 7M^4(Q^2 + t_1) + (Q^2 + t_1)(Q^4 + t_1^2 + Q^2t_1(2 + (y_2 - 4)y_2))$$

$$+ M^2(5Q^4 + 5t_1^2 + Q^2t_1(10 + y_2(3y_2 - 4)))) \cos(2(\varphi_1 - \varphi_2))\Big)M^2,$$

$$\overline{|\mathcal{A}(R + e \to e + \mathcal{H}[^3P_1^{(8)}]|^2} = \frac{512}{3}\pi^3\alpha^2\alpha_s e_Q^2 \frac{\langle\mathcal{O}^\mathcal{H}[^3P_1^{(8)}]\rangle}{M^5} \frac{1}{y_2^2 Q^2(M^2 + Q^2 + t_1)^4}$$

$$\times \Big((2 + (y_2 - 2)y_2)\big(Q^8 + t_1(M^2 + t_1)^2(2M^2 + t_1)\big)$$

$$+ 2Q^6(y_2 - 2)(M^2(y_2 - 2) - t_1(2 - y_2 + y_2^2))$$

$$+ Q^4(4M^2t_1(y_2 - 3)(y_2 - 2) + M^4(10 + (y_2 - 10)y_2) - 2t_1^2(y_2(6 + y_2(-5 + 2y_2)) - 6))$$

$$+ 2Q^2(M^4t_1(10 + (-8 + y_2)y_2) - 2M^6(y_2 - 1) - t_1^3(y_2 - 2)(2 + (y_2 - 1)y_2)$$

$$- M^2t_1^2(y_2(10 + y_2(2y_2 - 5)) - 12)) + 4Q\sqrt{t_1(1 - y_2)}(M^2 + Q^2 + t_1)(M^4(y_2 - 2)$$

$$+ (Q^2 + t_1)^2(y_2 - 2)y_2 - M^2(Q^2(2 + y_2) + t_1(2 + y_2 - 2y_2^2))) \cos(\varphi_1 - \varphi_2)$$

$$+ 2(y_2 - 1)((Q^2 + t_1)^4 - Q^2t_1(Q^2 + t_1)^2y_2^2 + M^4((Q^2 + t_1)^2 - 2Q^2t_1y_2) + 2M^2((Q^2 + t_1)^3$$

$$- Q^2t_1(Q^2 + t_1)y_2 - Q^2t_1^2y_2^2)) \cos(2(\varphi_1 - \varphi_2))\Big)M^2,$$

$$\overline{|\mathcal{A}(R + e \to e + \mathcal{H}[^3P_2^{(8)}]|^2} = \frac{512}{15}\pi^3\alpha^2\alpha_s e_Q^2 \frac{\langle\mathcal{O}^\mathcal{H}[^3P_2^{(8)}]\rangle}{M^5} \frac{1}{y_2^2 Q^2(M^2 + Q^2 + t_1)^4}$$

$$\times \Big((2 + (y_2 - 2)y_2)\big(Q^8 + (M^2 + t_1)^2(6M^4 + 6M^2t_1 + t_1^2)\big) + 2Q^6(M^2(8 + (y_2 - 8)y_2)$$

$$- t_1(y_2 - 3)(y_2 - 2)^2) + Q^4(M^4(38 + y_2(7y_2 - 38)) + 4M^2t_1(20 + y_2(8y_2 - 25))$$

$$+ t_1^2(44 - 2y_2(30 + y_2(2y_2 - 13)))) + 2Q^2(-(t_1^3(y_2 - 3)(y_2 - 2)^2) + 6M^6(3 + (y_2 - 3)y_2)$$

$$- M^2t_1^2(y_2(50 + y_2(6y_2 - 25)) - 40) - M^4t_1(y_2(52 + y_2(6y_2 - 25)) - 46))$$

$$+ 4Q\sqrt{t_1(1 - y_2)}(M^2 + Q^2 + t_1)(Q^4(4 + (y_2 - 2)y_2)$$

$$+ t_1^2(4 + (y_2 - 2)y_2) + 3M^4(2 + y_2(2y_2 - 3)) + M^2t_1(10 + y_2(6y_2 - 11))$$

$$+ Q^2(M^2(10 - 11y_2) + 2t_1(4 + (y_2 - 6)y_2))) \cos(\varphi_1 - \varphi_2)$$

$$- 2(y_2 - 1)(2M^2((Q^2 + t_1)^3 - 5Q^2t_1(Q^2 + t_1)y_2 + 3Q^2t_1^2y_2^2)$$

$$+ (Q^2 + t_1)^2(Q^4 + t_1^2 + Q^2 t_1(2 + (y_2 - 4)y_2))$$
$$+ M^4(Q^4 + t_1^2 + 2Q^2 t_1(1 + 3(y_2 - 1)y_2))) \cos\left(2(\varphi_1 - \varphi_2)\right)\Big)M^2. \tag{44}$$

As usual, $Q^2 = -q^2$ and $y_2 = (q \cdot P)/(k \cdot P)$, where P^μ, k^μ, k'^μ, and $q^\mu = k^\mu - k'^\mu$ are the four-momenta of the incoming proton, the incoming lepton, the outgoing lepton, and the virtual photon, respectively, φ_1 is the angle between $\mathbf{k}_{1T}$ and $\mathbf{p}_T$, and φ_2 is the angle between $\mathbf{q}_T$ and $\mathbf{p}_T$. The corresponding formulas in the collinear parton model [27] are recovered as explained in Eq. (36) and read:

$$\overline{|\mathcal{A}(g + e \to e + \mathcal{H}[^3S_1^{(8)}]|^2} = 0,$$
$$\overline{|\mathcal{A}(g + e \to e + \mathcal{H}[^1S_0^{(8)}]|^2} = 64\pi^3\alpha^2\alpha_s e_Q^2 \frac{\langle\mathcal{O}^\mathcal{H}[^1S_0^{(8)}]\rangle}{M} \frac{y_2^2 - 2y_2 + 2}{y_2^2 Q^2},$$
$$\overline{|\mathcal{A}(g + e \to e + \mathcal{H}[^3P_0^{(8)}]|^2} = \frac{256}{3}\pi^3\alpha^2\alpha_s e_Q^2 \frac{\langle\mathcal{O}^\mathcal{H}[^3P_0^{(8)}]\rangle}{M^3}$$
$$\times \frac{(y_2^2 - 2y_2 + 2)(Q^2 + 3M^2)^2}{y_2^2 Q^2 (Q^2 + M^2)^2},$$
$$\overline{|\mathcal{A}(g + e \to e + \mathcal{H}[^3P_1^{(8)}]|^2} = \frac{512}{3}\pi^3\alpha^2\alpha_s e_Q^2 \frac{\langle\mathcal{O}^\mathcal{H}[^3P_1^{(8)}]\rangle}{M^3}$$
$$\times \frac{((y_2^2 - 2y_2 + 2)Q^2 - 4(y_2 - 1))M^2}{y_2^2(Q^2 + M^2)^2},$$
$$\overline{|\mathcal{A}(g + e \to e + \mathcal{H}[^3P_2^{(8)}]|^2} = \frac{512}{15}\pi^3\alpha^2\alpha_s e_Q^2 \frac{\langle\mathcal{O}^\mathcal{H}[^3P_2^{(8)}]\rangle}{M^3}$$
$$\times \frac{((y_2^2 - 2y_2 + 2)(Q^4 + 6M^4) - 12(y_2 - 1)M^2Q^2)}{y_2^2 Q^2 (Q^2 + M^2)^2}. \tag{45}$$

Our analytic result for the $2 \to 3$ color-singlet subprocess (25) is rather lengthy, and we refrain from listing it here.

V. CHARMONIUM PRODUCTION AT THE TEVATRON

During the last decade, the CDF Collaboration at the Tevatron [28, 29] collected data on charmonium production at energies $\sqrt{S} = 1.8$ TeV (run I) and $\sqrt{S} = 1.96$ TeV (run II) in the central region of pseudorapidity $|\eta| < 0.6$. The data cover a large interval in transverse momentum, namely $5 < p_T < 20$ GeV (run I) and $0 < p_T < 20$ GeV (run II). The data sample of run I [28] includes p_T distributions of J/ψ mesons that were produced directly in the hard interaction, via radiative decays of χ_{cJ} mesons, via decays of ψ' mesons, and via decays of b hadrons. That of run II [29] includes p_T distributions of prompt J/ψ mesons, so

far without separation into direct, χ_{cJ}-decay, and ψ'-decay contributions, and of J/ψ mesons from b-hadron decays.

As is well known, the cross section of charmonium production measured at the Tevatron is more than one order of magnitude larger than the prediction of the CSM evaluated within the collinear parton model [30]. Switching from the collinear parton model to the k_T-factorization approach [20, 31, 32] somewhat ameliorates the situation, but still does not lead to agreement at all. On the other hand, a successful description of the data could be achieved with the NRQCD factorization formalism [1] implemented in the collinear parton model, including the fusion and fragmentation mechanisms of charmonium hadroproduction [33, 34].

Charmonium hadroproduction was studied some time ago using the NRQCD factorization formalism implemented in the k_T-factorization approach invoking both the fusion [20, 31, 32] and fragmentation pictures [10]. It was found [20, 31, 32] that, in order to describe the experimental data from the CDF Collaboration [28], it is necessary to employ a set of NMEs that greatly differs from the one favored by the collinear parton model. In this paper, we confirm this conclusion only to some degree.

On the other hand, the polarization of prompt J/ψ mesons measured at the Tevatron [35] also provides a sensitive probe of the NRQCD mechanism. This issue was carefully investigated both in the collinear parton model [36] and in the k_T-factorization approach [37]. None of these studies was able to prove or disprove the NRQCD factorization hypothesis.

In contrast to previous analyses in the collinear parton model or the k_T-factorization approach, we perform a joint fit to the run-I and run-II CDF data [28, 29] to obtain the color-octet NMEs for J/ψ, ψ', and χ_{cJ} mesons. We use three different versions of unintegrated gluon distribution function. Our calculations are based on exact analytical expressions for the relevant squared amplitudes, which were previously unknown in literature. Our fits include five experimental data sets, which come as p_T distributions of J/ψ mesons from direct production, prompt production, χ_{cJ} decays, and ψ' decays in run I and from prompt production in run II.

We now describe how to evaluate the differential hadronic cross section from Eq. (5) in combination with the squared matrix elements of the $2 \to 1$ and $2 \to 2$ subprocesses (20) and (21), respectively. The rapidity and pseudorapidity of a charmonium state with four-

momentum $p^\mu = (p^0, \mathbf{p}_T, p^3)$ are given by

$$y = \frac{1}{2} \ln \frac{p^0 + p^3}{p^0 - p^3}, \quad \eta = \frac{1}{2} \ln \frac{|\mathbf{p}| + p^3}{|\mathbf{p}| - p^3}, \tag{46}$$

respectively. For the $2 \to 1$ subprocess (20), we have

$$\frac{d\sigma^{\mathrm{KT}}(p + \overline{p} \to \mathcal{H} + X)}{d|\mathbf{p}_T|dy} = \frac{|\mathbf{p}_T|}{(|\mathbf{p}_T|^2 + M^2)^2} \int d|\mathbf{k}_{1T}|^2 \int d\varphi_1$$
$$\times \Phi_p(\xi_1, |\mathbf{k}_{1T}|^2, \mu^2) \Phi_{\overline{p}}(\xi_2, |\mathbf{k}_{2T}|^2, \mu^2) \overline{|\mathcal{A}(R + R \to \mathcal{H})|^2}, \tag{47}$$

where

$$\xi_1 = \frac{p^0 + p^3}{\sqrt{S}}, \qquad \xi_2 = \frac{p^0 - p^3}{\sqrt{S}}, \tag{48}$$

and $\mathbf{k}_{2T} = \mathbf{p}_T - \mathbf{k}_{1T}$. In our numerical analysis, we choose the factorization scale to be $\mu = M_T$. For the $2 \to 2$ subprocess (21), we have

$$\frac{d\sigma^{\mathrm{KT}}(p + \overline{p} \to \mathcal{H} + X)}{d|\mathbf{p}_T|dy} = \frac{|\mathbf{p}_T|}{(2\pi)^3} \int d|\mathbf{k}_{1T}|^2 \int d\varphi_1 \int dx_2 \int d|\mathbf{k}_{2T}|^2 \int d\varphi_2$$
$$\times \Phi_p(x_1, |\mathbf{k}_{1T}|^2, \mu^2) \Phi_{\overline{p}}(x_2, |\mathbf{k}_{2T}|^2, \mu^2) \frac{\overline{|\mathcal{A}(R + R \to \mathcal{H} + g)|^2}}{(x_2 - \xi_2)(2x_1 x_2 S)^2}, \tag{49}$$

where

$$x_1 = \frac{1}{(x_2 - \xi_2)S} \left[(\mathbf{k}_{1T} + \mathbf{k}_{2T} - \mathbf{p}_T)^2 - M^2 - |\mathbf{p}_T|^2 + x_2 \xi_1 S \right]. \tag{50}$$

We now present and discuss our results. In Table I, we list out fit results for the relevant color-octet NMEs for three different choices of unintegrated gluon distribution function, namely JB [11], JS [12], and KMR [13]. The color-singlet NMEs are not fitted, but determined from the measured partial decay widths of $\psi(nS) \to l^+ + l^-$ and $\chi_{c2} \to \gamma + \gamma$. The numerical values are adopted from Ref. [34] and read: $\langle \mathcal{O}^{J/\psi}[^3S_1^{(1)}] \rangle = 1.3$ GeV^3, $\langle \mathcal{O}^{\psi'}[^3S_1^{(1)}] \rangle = 6.5 \times 10^{-1}$ GeV^3, and $\langle \mathcal{O}^{\chi_{cJ}}[^3P_J^{(1)}] \rangle = (2J+1) \times 8.9 \times 10^{-2}$ GeV^5. They were obtained using the vacuum saturation approximation and heavy-quark spin symmetry in the NRQCD factorization formulas and including NLO QCD radiative corrections [38]. The relevant branching ratios are taken from Ref. [39] and read $B(J/\psi \to \mu^+ + \mu^-) = 0.0601$, $B(\psi' \to J/\psi + X) = 0.576$, $B(\chi_{c0} \to J/\psi + \gamma) = 0.012$, $B(\chi_{c1} \to J/\psi + \gamma) = 0.318$, and $B(\chi_{c2} \to J/\psi + \gamma) = 0.203$. They somewhat differ from the values used previously [40]. For comparison, we list in Table I also the NMEs obtained in Ref. [34] for the collinear parton model with the LO parton distribution functions of the proton by Martin, Roberts, Stirling, and Thorne (MRST98LO) [41].

18

We first study the relative importance of the different intermediate states in direct J/ψ and ψ' production. In previous fits to CDF data from run I [28], with $p_T > 5$ GeV, the linear combinations

$$M_r^{\mathcal{H}} = \langle \mathcal{O}^{\mathcal{H}}[^1S_0^{(8)}] \rangle + \frac{r}{m_c^2} \langle \mathcal{O}^{\mathcal{H}}[^3P_0^{(8)}] \rangle \tag{51}$$

for $\mathcal{H} = J/\psi, \psi'$ were fixed because it was infeasible to separate the contributions proportional to $\langle \mathcal{O}^{\mathcal{H}}[^1S_0^{(8)}] \rangle$ and $\langle \mathcal{O}^{\mathcal{H}}[^3P_0^{(8)}] \rangle$. By contrast, the new run-II data [28], which reach down to $p_T = 0$, allow us to determine $\langle \mathcal{O}^{\mathcal{H}}[^1S_0^{(8)}] \rangle$ and $\langle \mathcal{O}^{\mathcal{H}}[^3P_0^{(8)}] \rangle$ separately because the respective contributions exhibit different p_T dependences for $p_T < 5$ GeV. This feature is nicely illustrated in Fig. 1, where the shapes of the relevant color-octet contributions to prompt J/ψ production, proportional to $\langle \mathcal{O}^{\mathcal{H}}[^3S_1^{(8)}] \rangle$, $\langle \mathcal{O}^{\mathcal{H}}[^1S_0^{(8)}] \rangle$, and $\langle \mathcal{O}^{\mathcal{H}}[^3P_0^{(8)}] \rangle$, are compared with that of the CDF data from run II [29]. Notice that the color-octet contributions differ in the peak position, by up to 1 GeV. Apparently, this suffices to disentangle the contributions previously combined by Eq. (51). We find that $\langle \mathcal{O}^{J/\psi,\psi'}[^3P_0^{(8)}] \rangle$ and $\langle \mathcal{O}^{\psi'}[^1S_0^{(8)}] \rangle$ are compatible with zero, independent of the choice of unintegrated gluon density—a striking result. For the case of J/ψ production from ψ' decay, this implies that the $^3S_1^{(1)}$ and $^3S_1^{(8)}$ channels are sufficient to describe the measured p_T distribution (see Fig. 3).

In Figs. 2–5, we compare the CDF data on J/ψ mesons from direct production, ψ' decays, and χ_{cJ} decays in run I [28] and from prompt production in run II [29], respectively, with the theoretical results evaluated with the NMEs listed in Table I. From Fig. 2, we observe that the color-singlet contribution is significant, especially at low values of p_T, and comparable to the one from the $^1S_0^{(8)}$ channel. As is familiar from the collinear parton model, the $^3S_1^{(8)}$ contribution makes up the bulk of the cross section at large values of p_T. Incidentally, the values of $\langle \mathcal{O}^{J/\psi}[^3S_1^{(8)}] \rangle$ obtained in the k_T-factorization framework are in average quite close to the one obtained in the collinear parton model, as may be seen from Table I. The situation is very similar for J/ψ production from ψ' decay, considered in Fig. 3, except that the $^1S_0^{(8)}$ and $^3P_J^{(8)}$ contributions are negligible.

At this point, we wish to compare our results for direct J/ψ hadroproduction in the k_T-factorization approach with the literature, specifically with Refs. [20, 32], which consider the partonic subprocess (20). By contrast, in Ref. [31], the NLO subprocess $R + R \rightarrow J/\psi[^3S_1^{(8)}] + g$ was studied, leaving aside the LO subprocess (20). In Ref. [32], the value $\langle \mathcal{O}^{J/\psi}[^3S_1^{(8)}] \rangle = 7.0 \times 10^{-3}$ GeV^3 was obtained using the Kwiecinski-Martin-Stasto (KMS) [42] unintegrated gluon distribution function. This value is 2.6 times larger than the result

we found using the KMR [13] version, which is very similar to the KMS one. We attribute this difference in $\langle \mathcal{O}^{J/\psi}[^3S_1^{(8)}] \rangle$ to the different scale choice, $\mu = k_T$, used by the authors of Ref. [32]. Adopting their value for $\langle \mathcal{O}^{J/\psi}[^3S_1^{(8)}] \rangle$, we can reproduce their result for the respective cross section contribution. On the other hand, the value $\langle \mathcal{O}^{J/\psi}[^3S_1^{(8)}] \rangle = 15.0 \times 10^{-3}$ GeV^3 found in Ref. [20] exceeds the one of Ref. [32] by a factor of 2.1 and our KMR value by a factor of 5.6. Furthermore, the cross section evaluated in Ref. [20] falls off with p_T considerably more slowly than in Ref. [32] and here, only by one order of magnitude as p_T runs from 2 to 20 GeV, while the unintegrated gluon density in the proton falls off with k_T far more rapidly.

The discussion of J/ψ production from radiative χ_{cJ} decays, considered in Fig. 4, is simpler because there is only one free parameter in the fit, namely $\langle \mathcal{O}^{\chi_{c0}}[^3S_1^{(8)}] \rangle$. We confirm the conclusion of Ref. [31], that, in the k_T-factorization approach, the color-singlet contribution is sufficient to describe the data. In fact, the best fit is realized when $\langle \mathcal{O}^{\chi_{c0}}[^3S_1^{(8)}] \rangle$ is taken to be zero or very small. In case of the JB gluon density, the fitting procedure even favors a negative value of $\langle \mathcal{O}^{\chi_{c0}}[^3S_1^{(8)}] \rangle$.

In Fig. 5, the p_T distribution of prompt J/ψ production in run II is broken down into the contributions from direct production, ψ' decays, and χ_{cJ} decays. We observe that the latter is dominant for $p_T \lesssim 5$ GeV, while prompt J/ψ mesons are preferably produced directly at larger values of p_T. The contribution from ψ' decays stays at the level of several percent for all values of p_T. While the JS [12] and KMR [13] gluon densities allow for a faithful description of the measured p_T distribution [29], the JB [11] one has a problem in the low-p_T range, at $p_T \lesssim 5$ GeV, where even the χ_{cJ}-decay contribution, which is entirely of color-singlet origin, exceeds the data. This problem can be traced to the speed of growth of the JB gluon density as $k_T \to 0$. By contrast, the JS and KMR gluon densities are smaller and approximately k_T independent at low values of k_T. For this reason, we excluded the CDF prompt-J/ψ data from run I [28] and run II [29] from our fit based on the JB gluon density.

Considering the color-octet NMEs relevant for the J/ψ, ψ' and χ_{cJ} production mechanisms, we can formulate the following heuristic rule for favoured transitions from color-octet to color-singlet states: $\Delta L \simeq 0$ and $\Delta S \simeq 0$; *i.e.* these transitions are doubly chromoelectric and preserve the orbital angular momentum and the spin of the heavy-quark bound state.

VI. CHARMONIUM PRODUCTION AT HERA

At HERA, the cross section of prompt J/ψ production was measured in a wide range of the kinematic variables $W^2 = (P+q)^2$, $Q^2 = -q^2$, $y_2 = (P \cdot q)/(P \cdot k)$, $z = (P \cdot p)/(P \cdot q)$, p_T and y, where P^μ, k^μ, k'^μ, $q^\mu = k^\mu - k'^\mu$, and p^μ are the four-momenta of the incoming proton, incoming lepton, scattered lepton, virtual photon, and produced J/ψ meson, respectively, both in photoproduction [43], at small values of Q^2, and deep-inelastic scattering (DIS) [44], at large values of Q^2. At sufficiently large values of Q^2, the virtual photon behaves like a point-like object, while, at low values of Q^2, it can either act as a point-like object (direct photoproduction) or interact via its quark and gluon content (resolved photoproduction). Resolved photoproduction is only important at low values of z.

In the region $z \lesssim 1$, diffractive production, which is beyond the scope of this paper, takes place. In order to suppress the diffractive-production contribution, one usually applies the acceptance cut $z < 0.9$. This effectively eliminates the contributions from the $2 \rightarrow 1$ partonic subprocesses (22) and (24), so that we are left with the $2 \rightarrow 2$ partonic subprocesses (23) and (25).

Let us first present the relevant formulas for the double differential cross sections of DIS, direct photoproduction, and resolved photoproduction. In the case of DIS, we have

$$
\frac{d\sigma^{\mathrm{KT}}(p + e \rightarrow e + \mathcal{H} + X)}{d|\mathbf{p}_T|^2 dz} = \frac{1}{8z(2\pi)^5} \int dQ^2 \int dy_2 \int d|\mathbf{k}_{1T}|^2 \int d\varphi_1 \int d\varphi_2
$$
$$
\times \Phi_p(x_1, |\mathbf{k}_{1T}|^2, \mu^2) \frac{|\mathcal{A}(R + e \rightarrow e + \mathcal{H} + g)|^2}{(y_2 - \chi_2)(2x_1 S)^2}, \tag{52}
$$

where

$$
x_1 = \frac{1}{(y_2 - \chi_2)S} \left[(\mathbf{k}_{1T} + \mathbf{q}_{2T} - \mathbf{p}_T)^2 - M^2 - |\mathbf{p}_T|^2 + y_2\chi_1 S + (y_2 - \chi_2)Q^2 \right],
$$
$$
\chi_1 = \frac{p^0 + p^3}{2E_p}, \qquad \chi_2 = \frac{p^0 - p^3}{2E_e}. \tag{53}
$$

Here, E_p and E_e are the proton and lepton energies in the laboratory frame, and we have $S = 4E_p E_e$ and $|\mathbf{q}_{2T}| = \sqrt{(1 - y_2)Q^2}$.

In the case of direct photoproduction, we have

$$
\frac{d\sigma^{\mathrm{KT}}(p + e \rightarrow e + \mathcal{H} + X)}{d|\mathbf{p}_T|^2 dz} = \frac{1}{2z(2\pi)^2} \int dy_2 \int d|\mathbf{k}_{1T}|^2 \int d\varphi_1
$$
$$
\times \Phi_p(x_1, |\mathbf{k}_{1T}|^2, \mu^2) f_{\gamma/e}(y_2) \frac{|\mathcal{A}(R + \gamma \rightarrow \mathcal{H} + g)|^2}{y_2(y_2 - \chi_2)(2x_1 S)^2}, \tag{54}
$$

where

$$x_1 = \frac{1}{(y_2 - \chi_2)S} \left[(\mathbf{k}_{1T} - \mathbf{p}_T)^2 - M^2 - |\mathbf{p}_T|^2 + y_2\chi_1 S \right] \tag{55}$$

and $f_{\gamma/e}(y_2)$ is the quasi-real photon flux. In the Weizäcker-Williams approximation, the latter takes the form

$$f_{\gamma/e}(y_2) = \frac{\alpha}{2\pi} \left[\frac{1 + (1 - y_2)^2}{y_2} \ln \frac{Q_{max}^2}{Q_{min}^2} + 2m_e^2 y_2 \left(\frac{1}{Q_{min}^2} - \frac{1}{Q_{max}^2} \right) \right], \tag{56}$$

where $Q_{min}^2 = m_e^2 y_2^2/(1 - y_2)$ and Q_{max}^2 is determined by the experimental set-up, *e.g.* $Q_{max}^2 = 1\ \mathrm{GeV}^2$ [43].

In the case of resolved photoproduction, we take into account the $2 \to 1$ and $2 \to 2$ partonic subprocesses (20) and (21), respectively, where the first reggeized gluon comes from the proton and the second one from the photon. For subprocess (20), the relevant doubly differential cross section reads:

$$\frac{d\sigma^{\mathrm{KT}}(p + e \to e + \mathcal{H} + X)}{d|\mathbf{p}_T|^2 dz} = \frac{1}{2z(|\mathbf{p}_T|^2 + M^2)^2} \int dy_2 \int d|\mathbf{k}_{1T}|^2 \int d\varphi_1$$
$$\times \Phi_p(x_1, |\mathbf{k}_{1T}|^2, \mu^2) f_{\gamma/e}(y_2) \Phi_\gamma(x_2, |\mathbf{k}_{2T}|^2, \mu^2) \overline{|\mathcal{A}(R + R \to \mathcal{H})|^2}, \tag{57}$$

where

$$x_1 = \chi_1, \quad x_2 = \frac{\chi_2}{y_2}, \quad \mathbf{k}_{2T} = \mathbf{p}_T - \mathbf{k}_{1T}. \tag{58}$$

For subprocess (21), the relevant doubly differential cross section is given by

$$\frac{d\sigma^{\mathrm{KT}}(p + e \to e + \mathcal{H} + X)}{d|\mathbf{p}_T|^2 dz} = \frac{1}{2z(1 - z)(2\pi)^3} \int dy_2 \int d|\mathbf{k}_{1T}|^2 \int d\varphi_1 \int dx_2 \int d|\mathbf{k}_{2T}|^2 \int d\varphi_2$$
$$\times \Phi_p(x_1, |\mathbf{k}_{1T}|^2, \mu^2) f_{\gamma/e}(y_2) \Phi_\gamma(x_2, |\mathbf{k}_{2T}|^2, \mu^2) \frac{\overline{|\mathcal{A}(R + R \to \mathcal{H} + g)|^2}}{x_2(2x_1 x_2 y_2 S)^2}, \tag{59}$$

where

$$x_1 = \frac{1}{(x_2 y_2 - \chi_2)S} \left[(\mathbf{k}_{1T} - \mathbf{p}_T)^2 - M^2 - |\mathbf{p}_T|^2 + x_2 y_2 \chi_1 S \right]. \tag{60}$$

To evaluate the unintegrated gluon distribution function in the resolved photon, $\Phi_\gamma(x_2, |\mathbf{k}_{2T}|^2, \mu^2)$, we use a procedure suggested by Blümlein [45], which is similar to the proton case [11]. As input for this, we use the collinear parton distribution functions of the resolved photon by Glück, Reya, and Vogt (GRV$_\gamma$) [46].

In Figs. 6–9, our NRQCD predictions in the k_T-factorization approach, evaluated with the NMEs from Table I, are compared with the HERA data [43, 44]. Specifically, Figs. 6 and

7 refer to the p_T^2 and z distributions in photoproduction with $E_p = 820$ GeV, $E_e = 27.5$ GeV, 60 GeV $< W < 240$ GeV, and $Q^2 < 1$ GeV^2 [43], while Figs. 8 and 9 refer to those in DIS with $E_p = 920$ GeV, $E_e = 27.5$ GeV, 50 GeV $< W < 225$ GeV, and 2 GeV$^2 < Q^2 < 100$ GeV^2 [44]. Acceptance cuts common to both photoproduction and DIS include $p_T > 1$ GeV and $0.3 < z < 0.9$. In this regime, the LO NRQCD predictions in the k_T-factorization approach are mainly due to the color-singlet channels and are thus fairly independent of the color-octet NMEs presented in Table I. Therefore, our results agree well with previous calculations in the CSM [47], up to minor differences in the choice of the color-singlet NMEs and the c-quark mass.

VII.   CHARMONIUM PRODUCTION AT LEP2

Some time ago, the DELPHI Collaboration presented data on the inclusive cross section of J/ψ photoproduction in $\gamma\gamma$ collisions ($e^+ + e^- \rightarrow e^+ + e^- + J/\psi + X$) at LEP2, taken as a function of the J/ψ transverse momentum p_T [48]. The J/ψ mesons were identified through their decays to $\mu^+\mu^-$ pairs, and events where the system X contains a prompt photon were suppressed by requiring that at least four charged tracks were reconstructed. The average e^+e^- center-of-mass energy was $\sqrt{S} = 197$ GeV, the scattered positrons and electrons were antitagged, with maximum angle $\theta_{\mathrm{max}} = 32$ mrad, and the maximum $\gamma\gamma$ center-of-mass energy was chosen to be $W = 35$ GeV in order to reject the major part of the non-two-photon events.

Under LEP2 experimental conditions, most J/ψ mesons are produced promptly, while the cross section for J/ψ mesons from b-hadron decays is estimated to be about 1% of the total J/ψ cross section [49] and can be safely neglected. Because the average value of the photon virtuality Q^2 is small, the Weizsäcker-Williams approximation can be used to evaluate the e^+e^- cross section from the $\gamma\gamma$ cross section as

$$d\sigma(e^+ + e^- \rightarrow e^+ + e^- + \mathcal{H} + X) = \int dy_1 \int dy_2 \, f_{\gamma/e}(y_1) f_{\gamma/e}(y_2) d\sigma(\gamma + \gamma \rightarrow \mathcal{H} + X). \quad (61)$$

The process $e^+ + e^- \rightarrow e^+ + e^- + J/\psi + X$ receives contributions from direct, single-resolved, and double-resolved photoproduction. The relevant partonic subprocesses are: $\gamma + \gamma \rightarrow \mathcal{H}[^3S_1^{(8)}]+g$, $\gamma+R \rightarrow \mathcal{H}[^1S_0^{(8)}, {}^3P_J^{(8)}]$, $\gamma+R \rightarrow \mathcal{H}[^3S_1^{(1)}]+g$, $R+R \rightarrow \mathcal{H}[^3S_1^{(8)}, {}^1S_0^{(8)}, {}^3P_J^{(8)}]$, and $R + R \rightarrow \mathcal{H}[^3S_1^{(1)}] + g$. The squared amplitude of $\gamma + \gamma \rightarrow \mathcal{H}[^3S_1^{(8)}] + g$ may be found

in Ref. [49], the ones for the other partonic subprocesses were presented in Sec. IV.

The cross section of direct photoproduction is evaluated as

$$
\frac{d\sigma(e^+ + e^- \to e^+ + e^- + \mathcal{H} + X)}{d|\mathbf{p}_T|^2 dy} = \frac{1}{4\pi} \int dy_2 \, f_{\gamma/e}(y_1) f_{\gamma/e}(y_2)
$$
$$
\times \frac{y_1 y_2}{y_2 - \xi_2} \frac{\overline{|\mathcal{A}(\gamma + \gamma \to \mathcal{H} + g)|^2}}{(2y_1 y_2 S)^2},
\tag{62}
$$

where ξ_1 and ξ_2 are defined in Eq. (48) and

$$
y_1 = \frac{y_2 \xi_1 S - M^2}{(y_2 - \xi_2) S}.
\tag{63}
$$

In the case of single-resolved photoproduction via the $2 \to 1$ subprocesses, we have

$$
\frac{d\sigma^{\mathrm{KT}}(e^+ + e^- \to e^+ + e^- + \mathcal{H} + X)}{d|\mathbf{p}_T|^2 dy} = 4\pi \int dy_1 \, f_{\gamma/e}(y_1) f_{\gamma/e}(y_2)
$$
$$
\times \Phi_\gamma(x_1, |\mathbf{k}_{1T}|^2, \mu^2) y_2 \frac{\overline{|\mathcal{A}(R + \gamma \to \mathcal{H})|^2}}{(2x_1 y_1 y_2 S)^2},
\tag{64}
$$

where $x_1 = \xi_1/y_1$, $y_2 = \xi_2$, and $\mathbf{k}_{1T} = \mathbf{p}_T$. In the case of single-resolved photoproduction via the $2 \to 2$ subprocess, we have

$$
\frac{d\sigma^{\mathrm{KT}}(e^+ + e^- \to e^+ + e^- + \mathcal{H} + X)}{d|\mathbf{p}_T|^2 dy} = \frac{1}{2(2\pi)^2} \int dy_1 \int dy_2 \int d|\mathbf{k}_{1T}|^2 \int d\varphi_1 \, f_{\gamma/e}(y_1) f_{\gamma/e}(y_2)
$$
$$
\times \Phi_\gamma(x_1, |\mathbf{k}_{1T}|^2, \mu^2) \frac{y_2}{y_2 - \xi_2} \frac{\overline{|\mathcal{A}(R + \gamma \to \mathcal{H} + g)|^2}}{(2x_1 y_1 y_2 S)^2},
\tag{65}
$$

where

$$
x_1 = \frac{1}{y_1(y_2 - \xi_2)S} \left[(\mathbf{k}_{1T} - \mathbf{p}_T)^2 - M^2 - |\mathbf{p}_T|^2 + y_2 \xi_1 S \right].
\tag{66}
$$

In the case of double-resolved photoproduction via the $2 \to 1$ subprocesses, we have

$$
\frac{d\sigma^{\mathrm{KT}}(e^+ + e^- \to e^+ + e^- + \mathcal{H} + X)}{d|\mathbf{p}_T|^2 dy} = 2 \int dy_1 \int dy_2 \int d|\mathbf{k}_{1T}|^2 \int d\varphi_1 \, f_{\gamma/e}(y_1) f_{\gamma/e}(y_2)
$$
$$
\times \Phi_\gamma(x_1, |\mathbf{k}_{1T}|^2, \mu^2) \Phi_\gamma(x_2, |\mathbf{k}_{2T}|^2, \mu^2) \frac{\overline{|\mathcal{A}(R + R \to \mathcal{H})|^2}}{(2x_1 x_2 y_1 y_2 S)^2},
\tag{67}
$$

where $x_1 = \xi_1/y_1$, $x_2 = \xi_2/y_2$, and $\mathbf{k}_{2T} = \mathbf{p}_T - \mathbf{k}_{1T}$. In the case of double-resolved photo-production via the $2 \to 2$ subprocess, we have

$$
\frac{d\sigma^{\mathrm{KT}}(e^+ + e^- \to e^+ + e^- + \mathcal{H} + X)}{d|\mathbf{p}_T|^2 dy} = \frac{1}{2(2\pi)^3} \int dy_1 \int dy_2 \int d|\mathbf{k}_{1T}|^2 \int d\varphi_1
$$
$$
\times \int dx_2 \int d|\mathbf{k}_{2T}|^2 \int d\varphi_2 \, f_{\gamma/e}(y_1) \Phi_\gamma(x_1, |\mathbf{k}_{1T}|^2, \mu^2) f_{\gamma/e}(y_2) \Phi_\gamma(x_2, |\mathbf{k}_{2T}|^2, \mu^2)
$$
$$
\times \frac{y_2}{x_2 y_2 - \xi_2} \frac{\overline{|\mathcal{A}(R + R \to \mathcal{H} + g)|^2}}{(2x_1 x_2 y_1 y_2 S)^2},
\tag{68}
$$

24

where

$$x_1 = \frac{1}{y_1(x_2 y_2 - \xi_2)S} \left[(\mathbf{k}_{1T} + \mathbf{k}_{2T} - \mathbf{p}_T)^2 - M^2 - |\mathbf{p}_T|^2 + x_2 y_2 \xi_1 S \right]. \qquad (69)$$

In Fig. 10, we confront the p_T^2 distribution of $e^+ + e^- \to e^+ + e^- + J/\psi + X$, where X is devoid of prompt photons, measured by DELPHI [48] with our full theoretical prediction (line No. 4), which is broken down into the single-resolved color-octet contribution (line No. 1), the single-resolved color-singlet contribution (line No. 2), and the direct plus double-resolved contributions (line No. 3). We observe that the single-resolved contribution makes up the bulk of the cross section, while the direct and double-resolved contributions are greatly suppressed, and that, within the single-resolved contribution, the color-singlet channel is dominant. The experimental data overshoot the theoretical prediction by a moderate factor of 2–3. For the case of $\gamma\gamma$ collisions, we conclude that the color-singlet processes are dominant in the k_T-factorization approach, a situation familiar from photo- and electroproduction in ep collisions considered in Sec. VI. The situation is quite different for the collinear parton model, where color-octet processes dominate [49].

Recently, in Ref. [25], it was attempted to interpret the DELPHI data in the k_T-factorization approach invoking only the CSM and neglecting the cascade decays of the ψ' and χ_{cJ} mesons. Curve No. 2 in Fig. 10 approximately agrees with the corresponding predictions in Ref. [25] for $m_c = 1.55$ GeV. In Ref. [25], a significantly lower value of m_c is employed to reach agreement with the DELPHI data.

VIII.   CONCLUSION

Working at LO in the k_T-factorization approach to NRQCD, we analytically evaluated the squared amplitudes of prompt charmonium production by reggeized gluons in RR, $R\gamma$, and Re collisions. We extracted the relevant color-octet NMEs, $\langle \mathcal{O}^{\mathcal{H}}[^3S_1^{(8)}] \rangle$, $\langle \mathcal{O}^{\mathcal{H}}[^1S_0^{(8)}] \rangle$, and $\langle \mathcal{O}^{\mathcal{H}}[^3P_0^{(8)}] \rangle$ for $\mathcal{H} = J/\psi$, ψ', and χ_{cJ} through fits to p_T distributions measured by the CDF Collaboration in $p\bar{p}$ collisions at the Tevatron with $\sqrt{S} = 1.8$ TeV [28] and 1.96 TeV [29] using three different versions of unintegrated gluon distribution function, namely JB [11], JS [12], and KMR [13]. Appealing to the assumed NRQCD factorization, we used the NMEs thus obtained to predict various cross section distributions of prompt J/ψ photoproduction and electroproduction in ep collisions and photoproduction in e^+e^- collisions and compared them with ZEUS [43] and H1 [44] data from HERA and DELPHI [48] data from LEP2,

25

respectively. In the case of photoproduction, we included both the direct and resolved contributions. As for the unintegrated parton distribution functions of the proton and the resolved photon, we assumed the gluon content to be dominant.

Our fits to the Tevatron data turned out to be satisfactory, except for the one to the χ_{cJ} sample based on the JB gluon density in the proton, where the fit result significantly exceeded the measured cross section in the small-p_T region. We found agreement with the HERA and LEP2 data within a factor of 2, which is the typical size of the theoretical uncertainty due to the lack of knowledge of the precise value of the c-quark mass and the NLO corrections. Specifically, we found that direct and resolved photoproduction in ep collisions under HERA kinematic conditions dominantly proceed through color-singlet processes, namely $R(p) + \gamma \to \mathcal{H}[^3S_1^{(1)}] + g$ and $R(p) + R(\gamma) \to \mathcal{H}[^3S_1^{(1)}] + g$, respectively. Similarly, photoproduction in e^+e^- collisions under LEP2 kinematic conditions is mainly mediated via the color-singlet subprocess $R(\gamma) + \gamma \to \mathcal{H}[^3S_1^{(1)}] + g$, but the color-octet subprocess $R(\gamma) + \gamma \to \mathcal{H}[^1S_0^{(8)}]$ also contributes appreciably.

LO predictions in both the collinear parton model and the k_T-factorization framework suffer from sizeable theoretical uncertainties, which are largely due to unphysical-scale dependences. Substantial improvement can only be achieved by performing full NLO analyses. While the stage for the NLO NRQCD treatment of $2 \to 2$ processes has been set in the collinear parton model [50], conceptual issues still remain to be clarified in the k_T-factorization approach. Since, at NLO, incoming partons can gain a finite k_T kick through the perturbative emission of partons, one expects that essential features produced by the k_T-factorization approach at LO will thus automatically show up at NLO in the collinear parton model.

Acknowledgments

[1] G. T. Bodwin, E. Braaten, and G. P. Lepage, Phys. Rev. D **51**, 1125 (1995); **55**, 5853(E) (1997).

[2] CTEQ Collaboration, R. Brock *et al.*, Rev. Mod. Phys. **67**, 157 (1995).

[3] V. N. Gribov and L. N. Lipatov, Sov. J. Nucl. Phys. **15**, 438 (1972) [Yad. Fiz. **15**, 781 (1972)]; Yu. L. Dokshitzer, Sov. Phys. JETP **46**, 641 (1977) [Zh. Eksp. Teor. Fiz. **73**, 1216 (1977)]; G. Altarelli and G. Parisi, Nucl. Phys. **B126**, 298 (1977).

[4] E. A. Kuraev, L. N. Lipatov, and V. S. Fadin, Sov. Phys. JETP **44**, 443 (1976) [Zh. Eksp. Teor. Fiz. **71**, 840 (1976)]; I. I. Balitsky and L. N. Lipatov, Sov. J. Nucl. Phys. **28**, 822 (1978) [Yad. Fiz. **28**, 1597 (1978)].

[5] L. V. Gribov, E. M. Levin, and M. G. Ryskin, Phys. Rept. **100**, 1 (1983); S. Catani, M. Ciafoloni, and F. Hautmann, Nucl. Phys. **B366**, 135 (1991).

[6] J. C. Collins and R. K. Ellis, Nucl. Phys. **B360**, 3 (1991).

[7] L. N. Lipatov, Nucl. Phys. **B452**, 369 (1995).

[8] V. S. Fadin and L. N. Lipatov, Nucl. Phys. **B477**, 767 (1996).

[9] E. N. Antonov, L. N. Lipatov, E. A. Kuraev, and I. O. Cherednikov, Nucl. Phys. **B721**, 111 (2005).

[10] V. A. Saleev and D. V. Vasin, Phys. Rev. D **68**, 114013 (2003); Phys. Atom. Nucl. **68**, 94 (2005) [Yad. Fiz. **68**, 95 (2005)].

[11] J. Blümlein, Report No. DESY 95-121 (1995).

[12] H. Jung and G. P. Salam, Eur. Phys. J. C **19**, 351 (2001).

[13] M. A. Kimber, A. D. Martin, and M. G. Ryskin, Phys. Rev. D **63**, 114027 (2001).

[14] V. A. Saleev and D. V. Vasin, Phys. Lett. B **548**, 161 (2002).

[15] M. Ciafaloni, Nucl. Phys. **B296**, 49 (1988); S. Catani, F. Fiorani, and G. Marchesini, Phys. Lett. B **234**, 339 (1990); G. Marchesini, Nucl. Phys. **B445**, 49 (1995).

[16] V. G. Kartvelishvili, A. K. Likhoded, and S. R. Slabospitsky, Sov. J. Nucl. Phys. **28**, 678 (1978) [Yad. Fiz. **28**, 1315 (1978)]; S. S. Gershtein, A. K. Likhoded, and S. R. Slabospitsky, Sov. J. Nucl. Phys. **34**, 128 (1981) [Yad. Fiz. **34**, 227 (1981)]; E. L. Berger and D. Jones, Phys. Rev. D **23**, 1521 (1981); R. Baier and R. Rückl, Phys. Lett. B **102**, 364 (1981).

[17] W. Lucha, F. F. Schoberl, and D. Gromes, Phys. Rept. **200**, 127 (1991); E. J. Eichten and C. Quigg, Phys. Rev. D **52**, 1726 (1995).

[18] F. Maltoni, M. L. Mangano, and A. Petrelli, Nucl. Phys. **B519**, 361 (1998).

[19] J. H. Kühn, J. Kaplan, and E. G. O. Safiani, Nucl. Phys. **B157**, 125 (1979); B. Guberina, J. H. Kühn, R. D. Peccei, and R. Rückl, Nucl. Phys. **B174**, 317 (1980).

[20] S. P. Baranov, Phys. Rev. D **66**, 114003 (2002).

[21] V. S. Fadin, M. I. Kotsky, and L. N. Lipatov, Phys. Lett. B **415**, 97 (1997); D. Ostrovsky, Phys. Rev. D **62**, 054028 (2000).

[22] E. Braaten, K. Cheung, and T. C. Yuan, Phys. Rev. D **48**, 4230 (1993); E. Braaten and T. C. Yuan, Phys. Rev. D **50**, 3176 (1994); **52**, 6627 (1995); E. Braaten and J. Lee, Nucl. Phys. **B586**, 427 (2000).

[23] P. Cho and A. K. Leibovich, Phys. Rev. D **53**, 150 (1996); **53**, 6203 (1996).

[24] M. Cacciari and M. Kramer, Phys. Rev. Lett. **76**, 4128 (1996).

[25] A. V. Lipatov and N. P. Zotov, Eur. Phys. J. C **41**, 163 (2005).

[26] P. Ko, J. Lee, and H.S. Song, Phys. Rev. D **54**, 4312 (1996); **60**, 119902(E) (1996).

[27] S. Fleming and T. Mehen, Phys. Rev. D **57**, 1846 (1998).

[28] CDF Collaboration, F. Abe *et al.*, Phys. Rev. Lett. **79**, 572 (1997); **79**, 578 (1997); CDF Collaboration, T. Affolder *et al.*, Phys. Rev. Lett. **85**, 2886 (2000).

[29] CDF Collaboration, D. Acosta *et al.*, Phys. Rev. D **71**, 032001 (2005).

[30] M. Krämer, Prog. Part. Nucl. Phys. **47**, 141 (2001).

[31] Ph. Hägler, R. Kirschner, A. Schäfer, L. Szymanowski, and O. V. Teryaev, Phys. Rev. D **62**, 071502 (2000); Phys. Rev. Lett. **86**, 1446 (2001).

[32] F. Yuan and K.-T. Chao, Phys. Rev. D **63**, 034006 (2001); Phys. Rev. Lett. **87**, 022002 (2001).

[33] E. Braaten and S. Fleming, Phys. Rev. Lett. **74**, 3327 (1995); B. A. Kniehl and G. Kramer, Eur. Phys. J. C **6**, 493 (1999).

[34] E. Braaten, B. A. Kniehl, and J. Lee, Phys. Rev. D **62**, 094005 (2000).

[35] CDF Collaboration, T. Affolder *et al.*, Phys. Rev. Lett. **86**, 3963 (2001).

[36] B. A. Kniehl and J. Lee, Phys. Rev. D **62**, 114027 (2000); B. A. Kniehl, G. Kramer, and C. P. Palisoc, Phys. Rev. D **68**, 114002 (2003).

[37] F. Yuan and K.-T. Chao, Phys. Lett. B **500**, 99 (2001).

[38] R. Barbieri, R. Gatto, R. Kögerler, and Z. Kunszt, Phys. Lett. B **57**, 455 (1975); R. Barbieri,

M. Caffo, R. Gatto, and E. Remiddi, Nucl. Phys. **B192**, 61 (1981).

[39] Particle Data Group, S. Eidelman *et al.*, Phys. Lett. B **592**, 1 (2004).

[40] Particle Data Group, K. Hagiwara *et al.*, Phys. Rev. D **66**, 010001 (2002).

[41] A. D. Martin, R. G. Roberts, W. J. Stirling, and R. S. Thorne, Eur. Phys. J. C **4**, 463 (1998).

[42] J. Kwiecinski, A. D. Martin, and A. M. Stasto, Phys. Rev. D **56**, 3991 (1997).

[43] ZEUS Collaboration, S. Chekanov *et al.*, Eur. Phys. J. C **27**, 173 (2003).

[44] H1 Collaboration, C. Adloff *et al.*, Eur. Phys. J. C **25**, 41 (2002).

[45] J. Blümlein, Report No. DESY 95-125 (1995).

[46] M. Glück, E. Reya, and A. Vogt, Phys. Rev. D **46**, 1973 (1992).

[47] N. P. Zotov and V. A. Saleev, Phys. Atom. Nucl. **57**, 513 (1994) [Yad. Fiz. **57**, 543 (1994)]; V. A. Saleev and N. P. Zotov, Mod. Phys. Lett. A **9**, 151 (1994); V. A. Saleev, Phys. Rev. D **65**, 054041 (2002); N. P. Zotov and A. V. Lipatov, Phys. Atom. Nucl. **66**, 1760 (2003) [Yad. Fiz. **66**, 1807 (2003)].

[48] DELPHI Collaboration, J. Abdallah *et al.*, Phys. Lett. B **565**, 76 (2003).

[49] M. Klasen, B. A. Kniehl, L. N. Mihaila, and M. Steinhauser, Phys. Rev. Lett. **89**, 032001 (2002).

[50] M. Klasen, B. A. Kniehl, L. N. Mihaila, and M. Steinhauser, Nucl. Phys. **B609**, 518 (2001); **B713**, 487 (2005); Phys. Rev. D **71**, 014016 (2005).
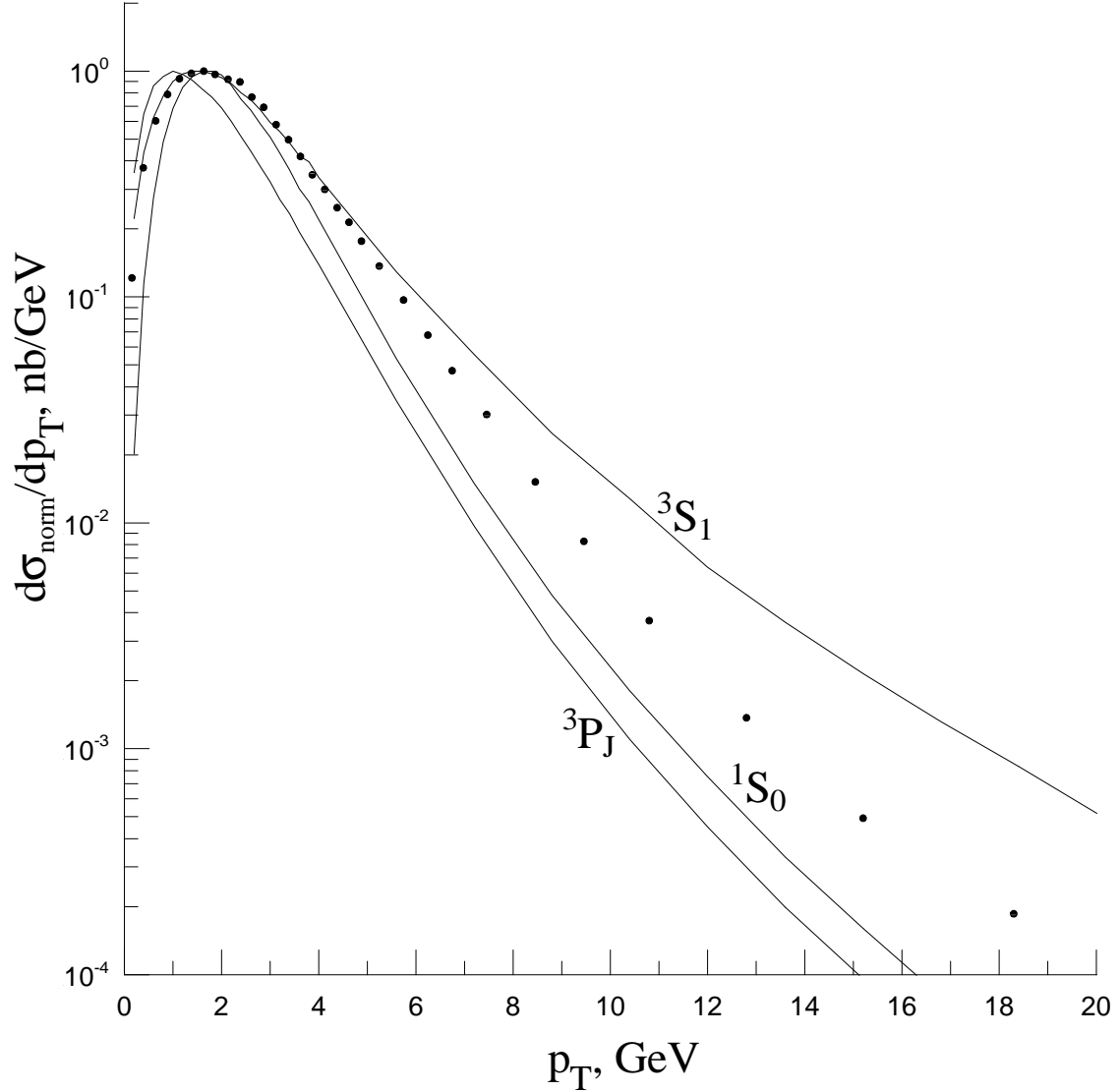
FIG. 1: Contributions to the p_T distribution of prompt J/ψ hadroproduction in $p\bar{p}$ scattering with $\sqrt{S} = 1.96$ TeV and $|y| < 0.6$ from the relevant color-octet states compared with CDF data from Tevatron run II [29]. All distributions are normalized to unity at their peaks.
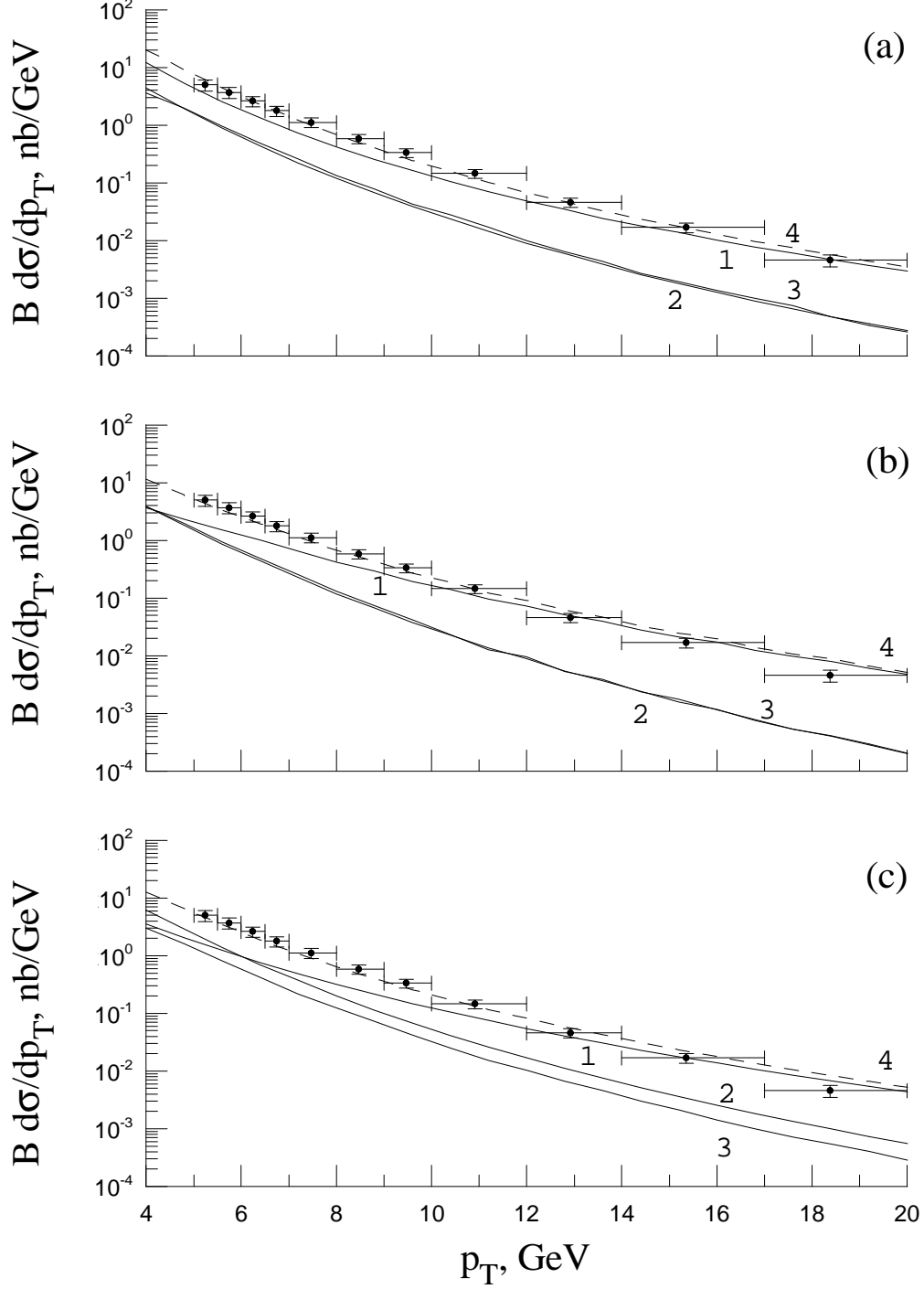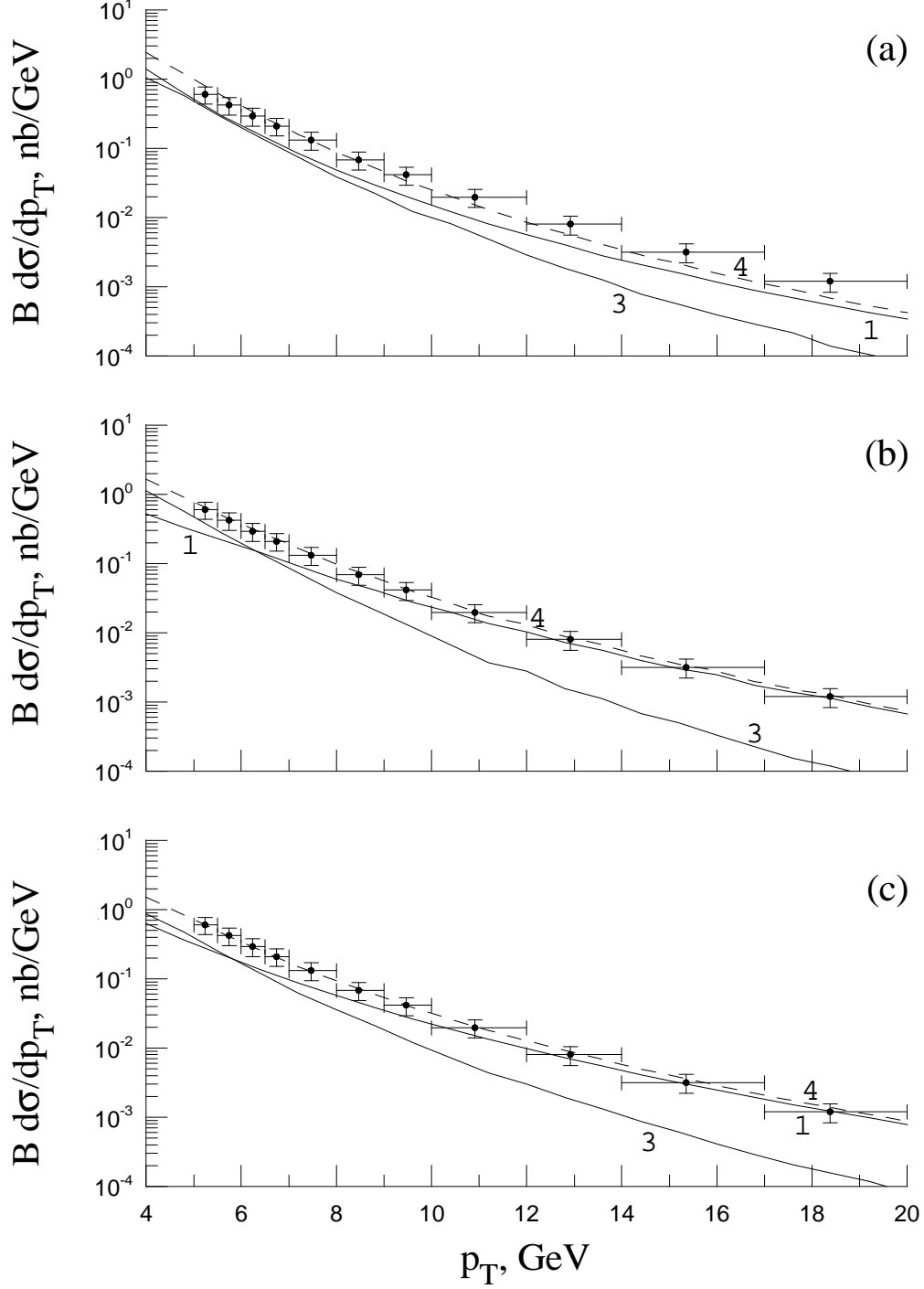
FIG. 2: Contributions to the p_T distribution of direct J/ψ hadroproduction in $p\bar{p}$ scattering with $\sqrt{S} = 1.8$ TeV and $|y| < 0.6$ from the partonic subprocesses (1) $R + R \to J/\psi[^3S_1^{(8)}]$, (2) $R + R \to J/\psi[^1S_0^{(8)}, ^3P_J^{(8)}]$, (3) $R + R \to J/\psi[^3S_1^{(1)}] + g$, and (4) their sum compared with CDF data from Tevatron run I [28]. The theoretical results are obtained with the (a) JB [11], (b) JS [12], or (c) KMR [13] unintegrated gluon distribution functions. The decay branching fraction $B(J/\psi \to \mu^+ + \mu^-)$ is included.

31

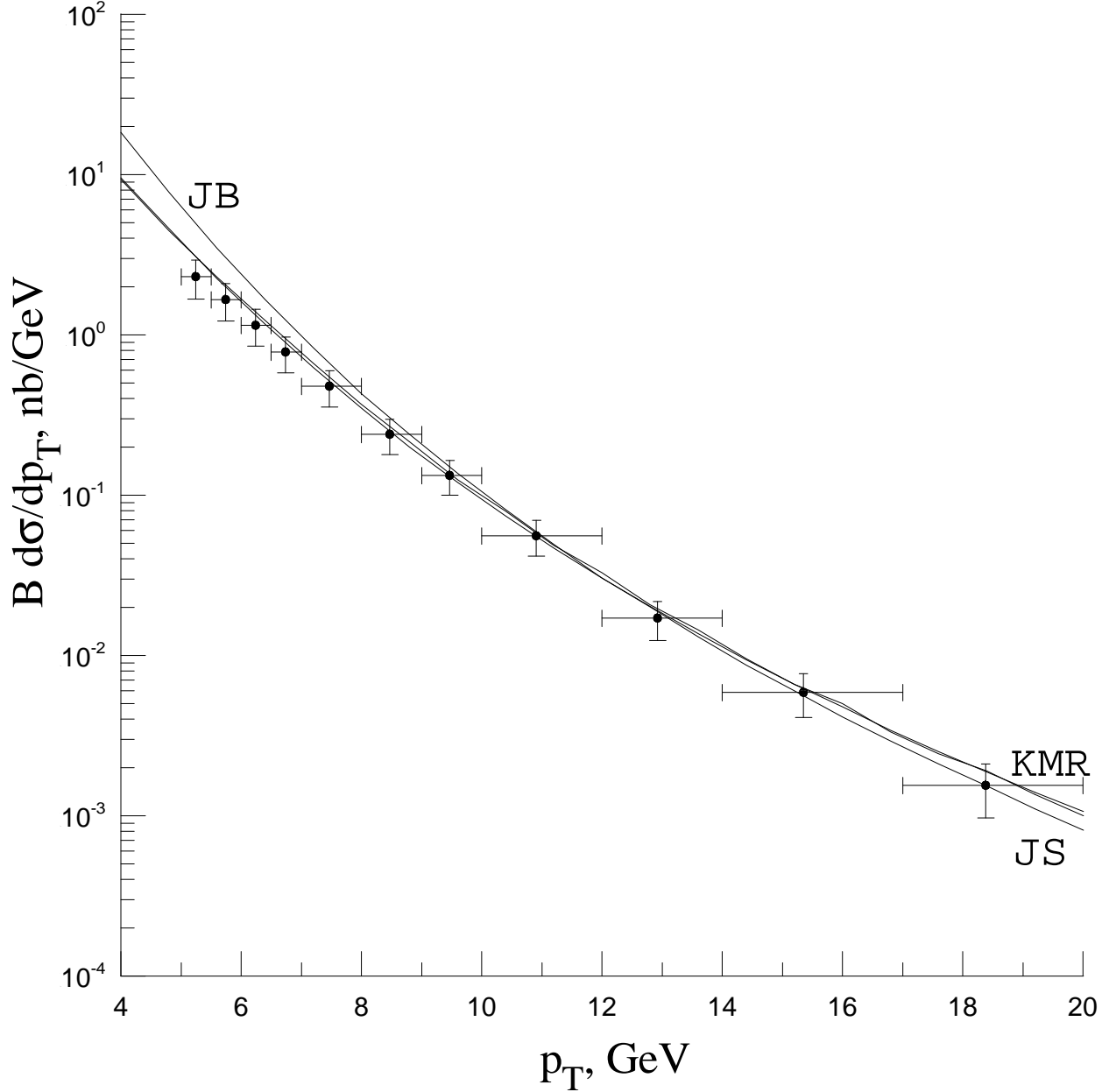FIG. 3: Contributions to the p_T distribution of J/ψ mesons from ψ' decays in hadroproduction in $p\overline{p}$ scattering with $\sqrt{S} = 1.8$ TeV and $|y| < 0.6$ from the partonic subprocesses (1) $R+R \to \psi'[^3S_1^{(8)}]$, (2) $R+R \to \psi'[^1S_0^{(8)}, {}^3P_J^{(8)}]$ (this contribution actually vanished), (3) $R+R \to \psi'[^3S_1^{(1)}]+g$, and (4) their sum compared with CDF data from Tevatron run I [28]. The theoretical results are obtained with the (a) JB [11], (b) JS [12], or (c) KMR [13] unintegrated gluon distribution functions. The decay branching fraction $B(J/\psi \to \mu^+ + \mu^-)$ is included.

32

FIG. 4: Contributions to the p_T distribution of J/ψ mesons from χ_{cJ} decays in hadroproduction in $p\bar{p}$ scattering with $\sqrt{S} = 1.8$ TeV and $|y| < 0.6$ from the sum of the partonic subprocesses $R+R \to \chi_{cJ}[^3P_J^{(1)}]$ and $R+R \to \chi_{cJ}[^3S_1^{(8)}]$, the latter of which being quite unimportant, compared with CDF data from Tevatron run I [28]. The theoretical results are obtained with the JB [11], JS [12], or KMR [13] unintegrated gluon distribution functions. The decay branching fraction $B(J/\psi \to \mu^+ + \mu^-)$ is included.

33
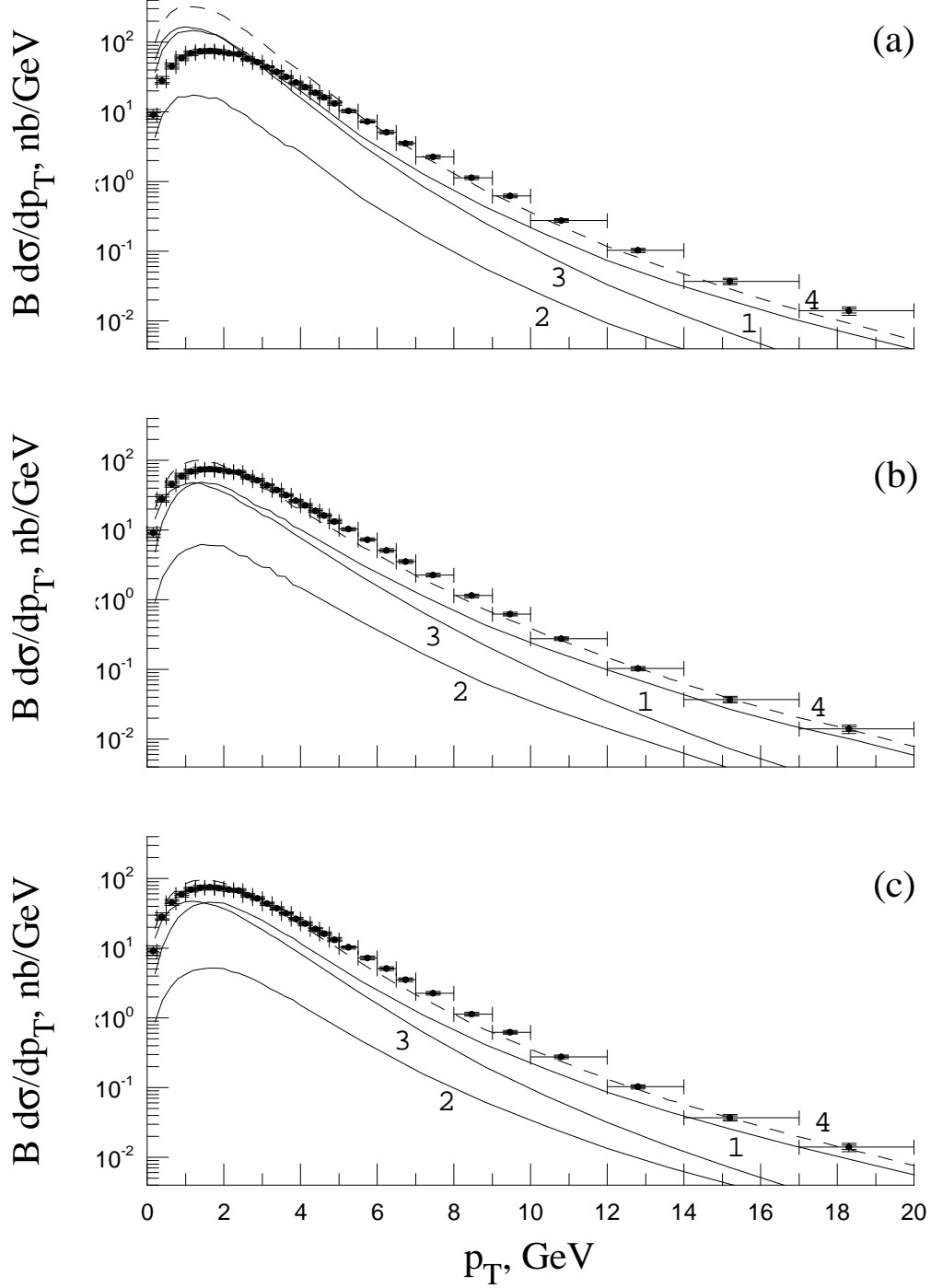
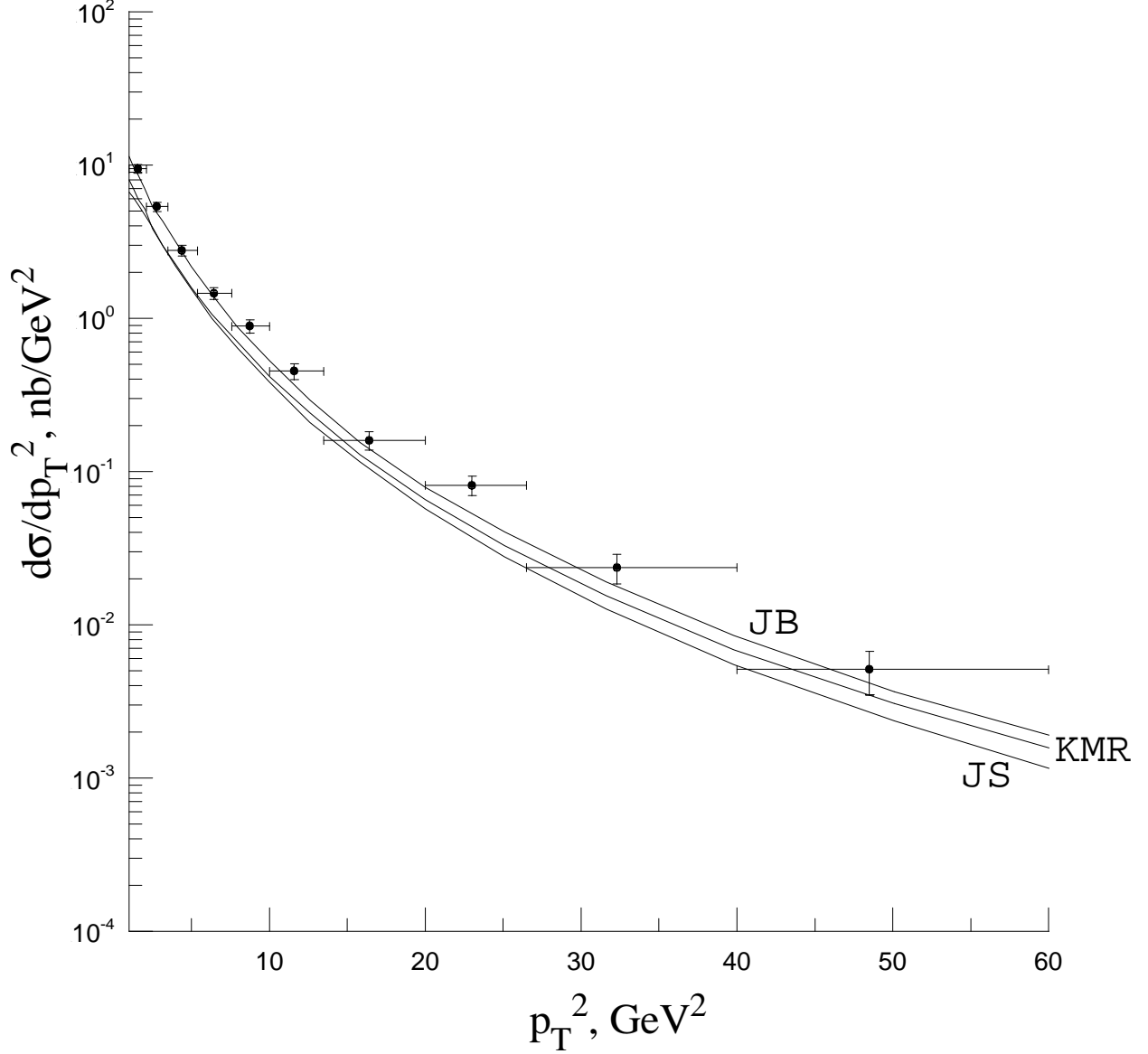FIG. 5: Contributions to the p_T distribution of prompt J/ψ hadroproduction in $p\bar{p}$ scattering with $\sqrt{S} = 1.96$ TeV and $|y| < 0.6$ from (1) direct production, (2) ψ' decays, (3) χ_{cJ} decays, and (4) their sum compared with CDF data from Tevatron run II [29]. The theoretical results are obtained with the (a) JB [11], (b) JS [12], or (c) KMR [13] unintegrated gluon distribution functions. The decay branching fraction $B(J/\psi \to \mu^+ + \mu^-)$ is included.

FIG. 6: Contribution to the p_T^2 distribution of prompt J/ψ photoproduction in ep scattering with $E_p = 820$ GeV, $E_e = 27.5$ GeV, 60 GeV $< W < 240$ GeV, $Q^2 < 1$ GeV^2, and $0.3 < z < 0.9$ from the direct-photon subprocess $R + \gamma \to \mathcal{H}[^3S_1^{(1)}] + g$ compared with ZEUS data from HERA [43]. The resolved-photon subprocesses $R + R \to \mathcal{H}[^3S_1^{(1)}, {}^3P_J^{(1)}, {}^3S_1^{(8)}, {}^1S_0^{(8)}, {}^3P_J^{(8)}]$ are neglected. The theoretical results are obtained with the JB [11], JS [12], or KMR [13] unintegrated gluon distribution functions.
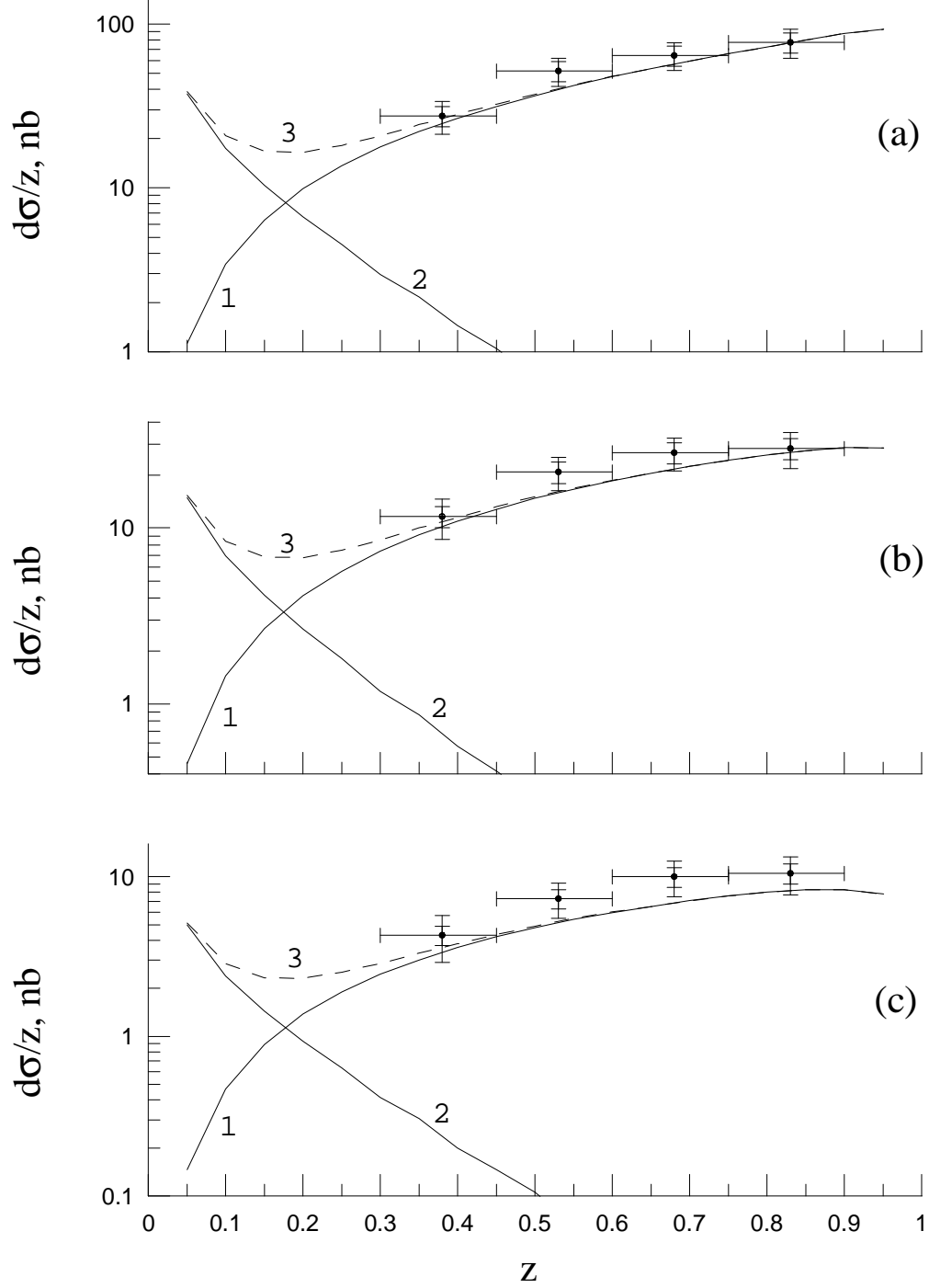
FIG. 7: Contributions to the z distribution of prompt J/ψ photoproduction in ep scattering with $E_p = 820$ GeV, $E_e = 27.5$ GeV, 60 GeV $< W < 240$ GeV, $Q^2 < 1$ GeV^2, and (a) $p_T > 1$ GeV, (b) $p_T > 2$ GeV, or (c) $p_T > 3$ GeV from (1) the direct-photon subprocess $R + \gamma \rightarrow \mathcal{H}[^3S_1^{(1)}] + g$, (2) the resolved-photon subprocesses $R + R \rightarrow \mathcal{H}[^3S_1^{(1)}, {}^3P_J^{(1)}, {}^3S_1^{(8)}, {}^1S_0^{(8)}, {}^3P_J^{(8)}]$, and (3) their sum compared with ZEUS data from HERA [43]. The theoretical results are obtained with the JB [11] unintegrated gluon distribution function.
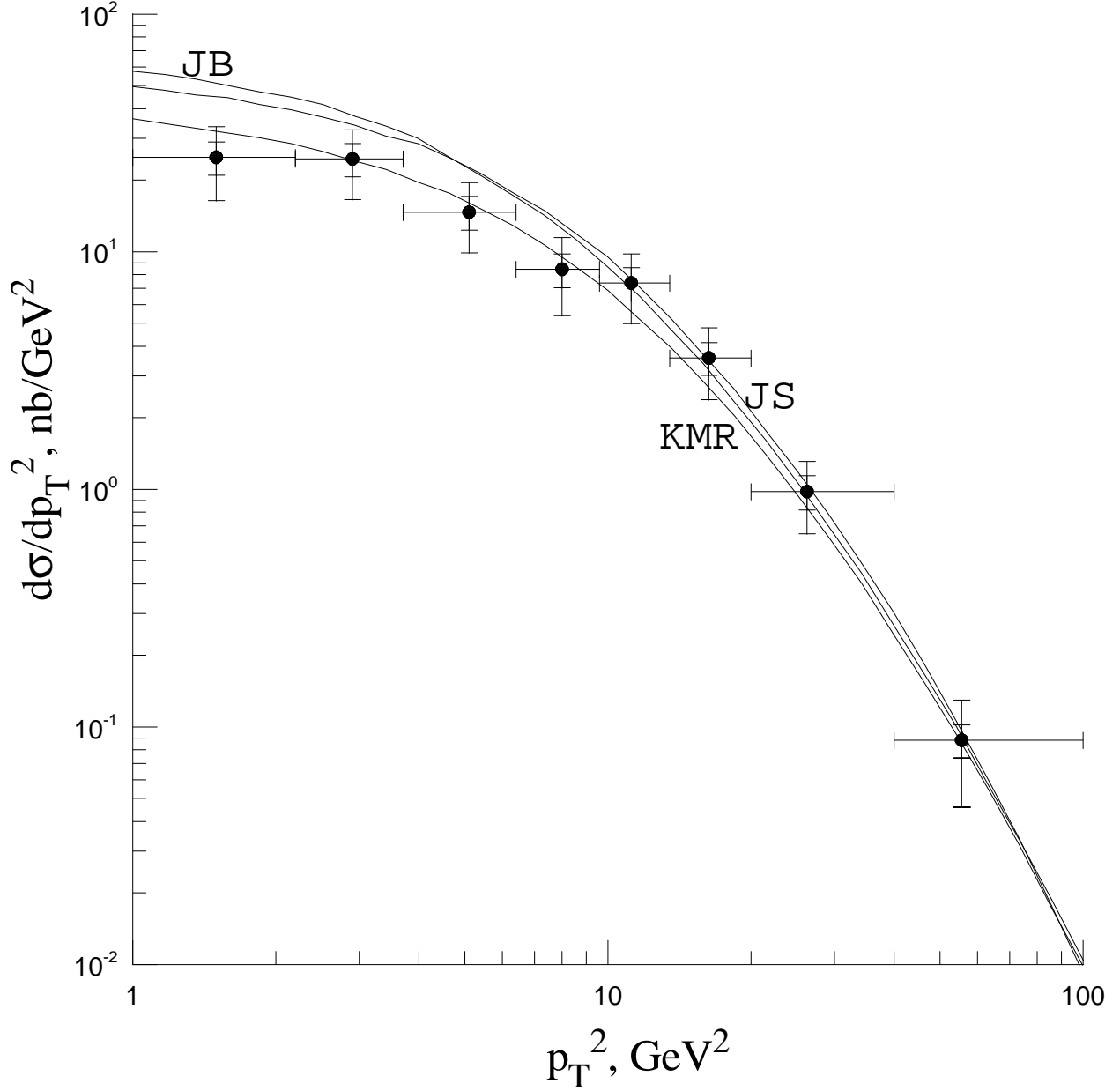
36

FIG. 8: Contribution to the p_T^2 distribution of prompt J/ψ electroproduction in ep scattering with $E_p = 920$ GeV, $E_e = 27.5$ GeV, 50 GeV $< W < 225$ GeV, 2 GeV$^2 < Q^2 < 100$ GeV^2, and $0.3 < z < 0.9$ from the color-singlet subprocess $R + e \rightarrow e + \mathcal{H}[^3S_1^{(1)}] + g$ compared with H1 data from HERA [44]. The theoretical results are obtained with the JB [11], JS [12], or KMR [13] unintegrated gluon distribution functions.
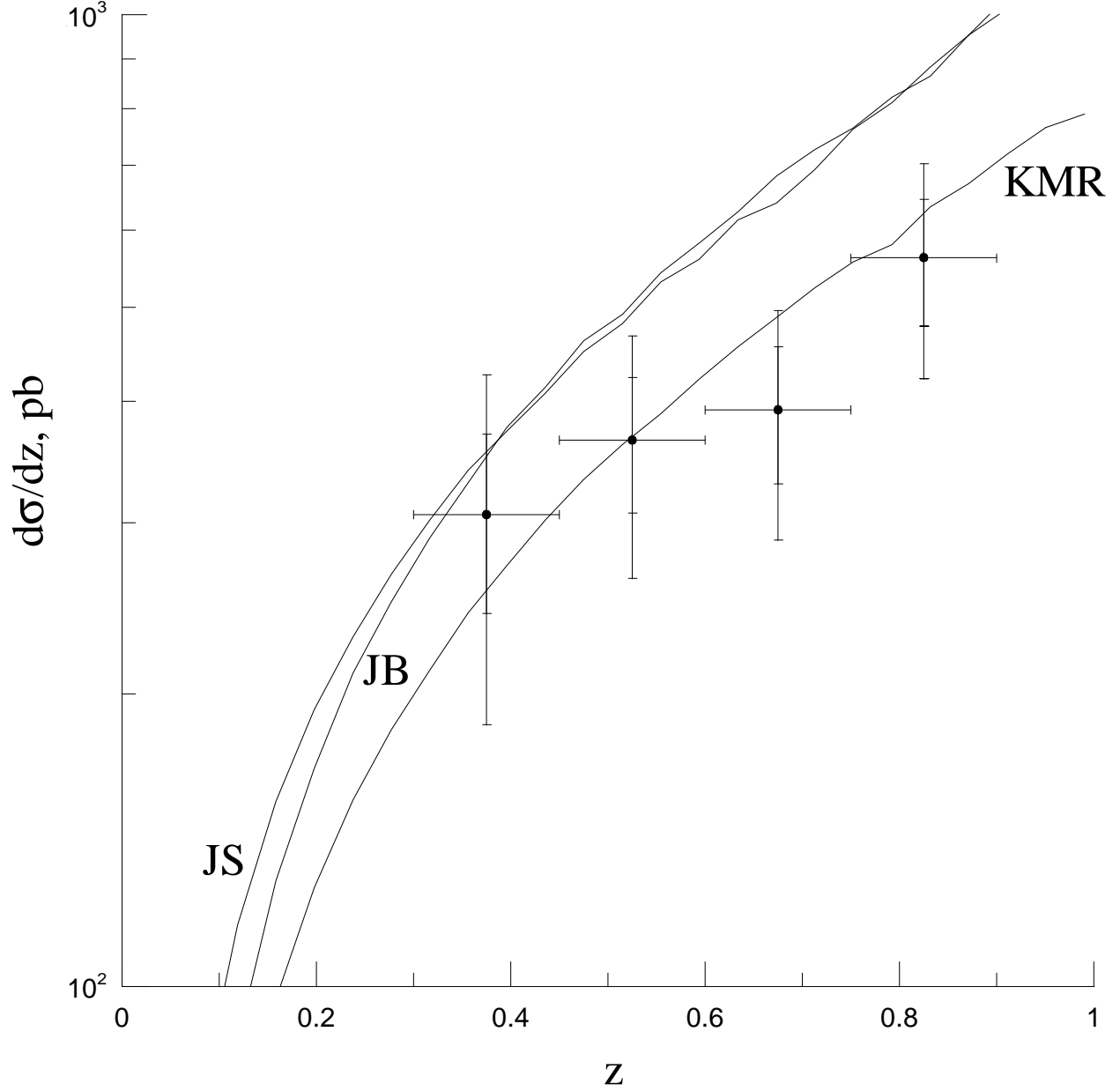
FIG. 9: Contribution to the z distribution of prompt J/ψ electroproduction in ep scattering with $E_p = 920$ GeV, $E_e = 27.5$ GeV, 50 GeV $< W <$ 225 GeV, 2 GeV$^2 < Q^2 <$ 100 GeV^2, and $p_T > 1$ GeV from the color-singlet subprocess $R + e \rightarrow e + \mathcal{H}[^3S_1^{(1)}] + g$ compared with H1 data from HERA [44]. The theoretical results are obtained with the JB [11], JS [12], or KMR [13] unintegrated gluon distribution functions.
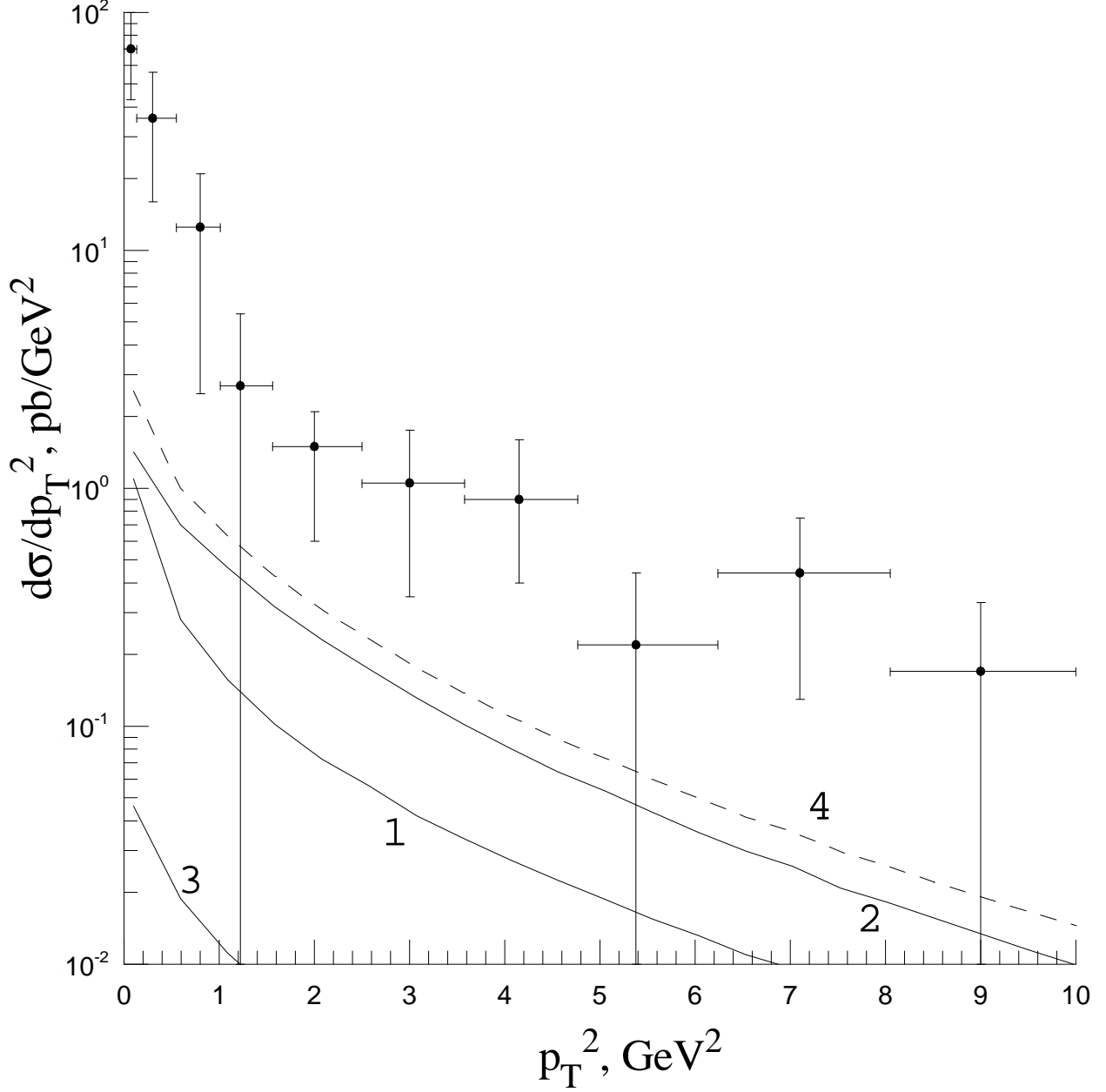
FIG. 10: Contributions to the p_T^2 distribution of prompt J/ψ photoproduction in e^+e^- annihilation with $\sqrt{S} = 197$ GeV, $Q^2 < 9.93$ GeV^2, $W < 35$ GeV, and $|y| < 2$ from the partonic subprocesses (1) $R + \gamma \to \mathcal{H}[^1S_0^{(8)}, ^3P_J^{(8)}]$, (2) $R + \gamma \to \mathcal{H}[^3S_1^{(1)}] + g$, (3) $\gamma + \gamma \to \mathcal{H}[^3S_1^{(8)}] + g$, $R + R \to \mathcal{H}[^3S_1^{(8)}, ^1S_0^{(8)}, ^3P_J^{(8)}]$, and $R + R \to \mathcal{H}[^3S_1^{(1)}] + g$, and (4) their sum compared with DELPHI data from LEP2 [48]. The theoretical results are obtained with the JB [11] unintegrated gluon distribution function.

39

TABLE I: NMEs for J/ψ, ψ', and χ_{cJ} mesons from fits in the collinear parton model (PM) [34] using the MRST98LO parton distribution functions of the proton [41] and in the k_T-factorization approach using the JB [11], JS [12], and KMR [13] unintegrated gluon distribution functions. The CDF prompt data from run I [28] and run II [29] have been excluded from our fit based on the JB gluon density.

NME	PM [34]	Fit JB	Fit JS	Fit KMR
$\langle \mathcal{O}^{J/\psi}[^3S_1^{(1)}]\rangle/\mathrm{GeV}^3$	1.3	1.3	1.3	1.3
$\langle \mathcal{O}^{J/\psi}[^3S_1^{(8)}]\rangle/\mathrm{GeV}^3$	4.4×10^{-3}	1.5×10^{-3}	6.1×10^{-3}	2.7×10^{-3}
$\langle \mathcal{O}^{J/\psi}[^1S_0^{(8)}]\rangle/\mathrm{GeV}^3$	—	6.6×10^{-3}	9.0×10^{-3}	1.4×10^{-2}
$\langle \mathcal{O}^{J/\psi}[^3P_0^{(8)}]\rangle/\mathrm{GeV}^5$	—	0	0	0
$M_{3.4}^{J/\psi}/\mathrm{GeV}^3$	8.7×10^{-2}	6.6×10^{-3}	9.0×10^{-3}	1.4×10^{-2}
$\langle \mathcal{O}^{\psi'}[^3S_1^{(1)}]\rangle/\mathrm{GeV}^3$	6.5×10^{-1}	6.5×10^{-1}	6.5×10^{-1}	6.5×10^{-1}
$\langle \mathcal{O}^{\psi'}[^3S_1^{(8)}]\rangle/\mathrm{GeV}^3$	4.2×10^{-3}	3.0×10^{-4}	1.5×10^{-3}	8.3×10^{-4}
$\langle \mathcal{O}^{\psi'}[^1S_0^{(8)}]\rangle/\mathrm{GeV}^3$	—	0	0	0
$\langle \mathcal{O}^{\psi'}[^3P_0^{(8)}]\rangle/\mathrm{GeV}^5$	—	0	0	0
$M_{3.5}^{\psi'}/\mathrm{GeV}^3$	1.3×10^{-2}	0	0	0
$\langle \mathcal{O}^{\chi_{c0}}[^3P_0^{(1)}]\rangle/\mathrm{GeV}^5$	8.9×10^{-2}	8.9×10^{-2}	8.9×10^{-2}	8.9×10^{-2}
$\langle \mathcal{O}^{\chi_{c0}}[^3S_1^{(8)}]\rangle/\mathrm{GeV}^3$	2.3×10^{-3}	0	2.2×10^{-4}	4.7×10^{-5}
$\chi^2/\mathrm{d.o.f}$	—	2.2	4.1	3.0